Instrument Familiarization Plan for ground based observations of SPSS. III. Second Order Contamination and Polarization Effects

prepared by: G. Altavilla, S. Ragaini, E. Pancino, G. Cocozza, M. Bellazzini, S. Galleti, S. Marinoni
approved by: F. van Leeuwen
authorized by: M.G. Lattanzi
reference: GAIA-C5-TN-OABO-GA-005-1
issue: 1
revision: 0
date: 2014-03-10
status: Issued

Abstract

The main goal of the astronomical data reduction is the removal of the instrumental signatures such as the bias offset, the dark current effect and the varying pixel to pixel sensitivity, to cite the most common instrumental features. Less common but more complex effects are the second order contamination and the instrumental polarization. In this document we focus on these two aspects, from the spectroscopic point of view.

Document History

Issue	Revision	Date	Author	Comment
1	0	10-Mar-2014	FVL, GA	Typos corrected. History corrected, issued.
D	10	09-Jan-2014	GA	minor corrections.
D	9	09-Dec-2013	GA	SR comments included.
D	8	22-Nov-2013	GA	EP comments included.
D	7	30-Oct-2013	GA	new polarization test at TNG included. Dicussion on the possible LRB sec. ord. contamination.
D	6	11-Jun-2013	GA	revised treatment of the airmass in the sec order correction; DOLores and EFOSC2 2nd ord figures revised;
D	5	5-Nov-2012	GA	effective airmass included in FIG 9, but negligible.
D	4	19-Oct-2012	GA	heliocentric velocity correction for 2nd order correction discussed; second order correction tested on a second run for TNG; second order correction tested on 2 more runs for NTT.
D	3	09-May-2012	GA	AB & EP comments included, general revision and additions.
D	2	15-Feb-2012	GA	JMC comments inlcuded, authors list revised.
D	1	20-Jan-2012	GA	First version, doc started on Aug 31 2011.

Acronyms list

The following table has been generated from the on-line Gaia acronym list:

Acronym	Description
ADU	Analogue-to-Digital Unit
BFOSC	Bologna Faint Object Spectrograph & Camera
CAFOS	Calar Alto Faint Object Spectrograph
CAHA	Centro Astronómico Hispano Alemán
CCD	Charge-Coupled Device
DOLORES	Device Optimized for LOw REsolution Spectroscopy
EFOSC2	ESO Faint Object Spectrograph & Camera
ESO	European Southern Observatory
FWHM	Full Width at Half-Maximum
IRAF	Image Reduction and Analysis Facility
NOAO	National Optical Astronomy Observatories
NTT	New Technology Telescope
REM	Rapid-Eye Mount

REMIR	REM IR camera
ROSS	REM Optical Slitless Spectrograph
RUCA	Rueda Cachanilla
SPM	San Pedro Mártir Observatory
SPSS	Spectro-Photometric Standard Star
TNG	Telescopio Nazionale Galileo

Contents

1 Introduction

The results reported in this document must be considered, together with the results about the CCD shutter characterization and linearity evaluation (GA-004) when observing with a given instrument and when reducing the corresponding data. For this reason the present document is complementary to the observations protocols (EP-001, EP-003) and to the data reduction and quality control protocols related to our observational campaign (SMR-001, SMR-002, SMR-003, SMR-004).

1.1 Second order contamination

Low resolution spectrographs and large format CCDs allow observations of a wide wavelength range ($\simeq$3300–10000 Å). If we consider a transmission grating as dispersing element, the grating equation is

$$m\lambda = \sigma(\sin\beta \pm \sin\alpha) \tag{1}$$

where m is the order number, σ the distance between the grooves, α and β the angles of incidence and diffraction, respectively, measured from the normal to the grating surface. The plus sign in eq. 1 applies to a reflection grating, the minus sign to a transmission grating (Schroeder, 2000). Eq. 1 shows e.g. that λ_1 at first order ($m = 1$) can overlap with a shorter wavelength λ_2 at second order ($m = 2$) if $\lambda_1 = 2 \times \lambda_2$ (with a real instrument the m coefficient is practically two but a very small shift, a few times 10Å, may occurr, Gutierrez-Moreno et al. 1994). More in general, overlap appears if $\lambda_{m1} = \frac{m2}{m1} \times \lambda_{m2}$ where $m1$ and $m2$ are different orders. Different dispersing elements, such as grisms, are described by more complicate equations (Traub, 1990), but the concept of the order contamination is the same. A grism dispersion equation involving first and second order spectra may be described by a relation as

$$\lambda_{1st\ order} = a \times \lambda_{2nd\ order} + b \tag{2}$$

(see Szokoly et al. 2004). If no additional device is used, such as cross-disperser elements or second order blocking filters[1], spectra of different orders (usually the first and the second) may partially overlap. The contaminated range depends on the optical characteristics of the instrument but the intensity of the contamination depends also on the spectral shape of the observed source (typically grism spectra of blue sources are more contaminated than red sources spectra). Fig. 1 shows a 2D spectrum of LTT1020 observed at high zenithal distance, where first and second order spectra are relatively well separated thanks to atmospheric diffraction. When the atmosphere acts as a cross-disperser, the comparison of spectral features in the two orders allows to determine the function that maps the first order light into the second.

Two of the instruments involved in our campaign (see GA-002 and LF-001 for more details) to define the list of SpectroPhotometric Standard Stars (SPSS, see GA-001 and GA-003) significantly suffer from this problem in their low-resolution red grisms spectra:

[1]Blue light blocking filters that cancel out or greatly reduce the contribution of the blue edge of the second order spectrum on the red edge of the first order spectrum.

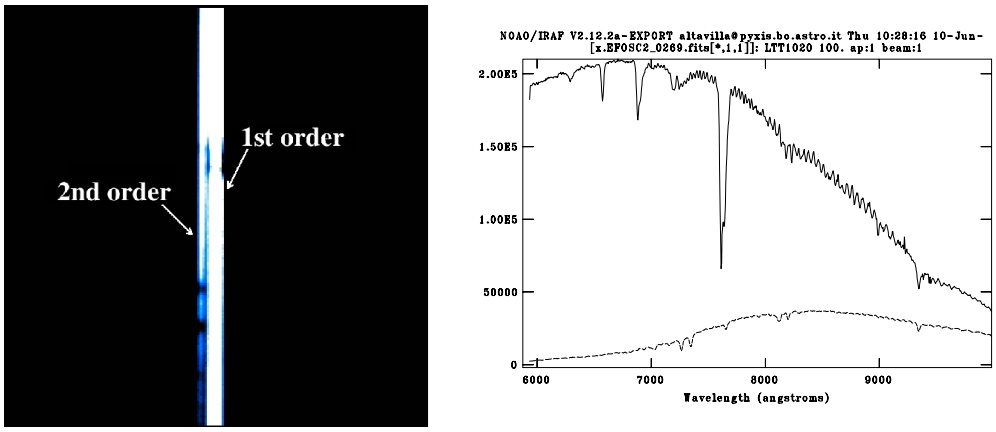

FIGURE 1: Left: detail of a Gr#16, 10" slit spectrum of LTT1020 observed with EFOSC2@NTT at airmass $\simeq 1.92$. Due to the large atmospheric refraction that acts as a cross disperser, the second order spectrum is relatively well separated from the first order spectrum and is evident on the left of the main bright spectrum. Right: one-dimensional extraction of the whole spectrum shown on the left and of the faint second order only (dashed line).

- the LR-R grism available at DOLoRes@TNG covers the range 4470–10070 Å and it has a built-in order-blocking filter cutting blueward of $\simeq 5000$ Å. Nevertheless, spectra are affected by second order contamination, which is evident especially in blue stars spectra, starting around 9500 Å[2]. The LR-B grism was not expected to be affected by second order contamination, nevertheless it shows peculiarities that mimic or can be easily explained by second order contamination (Sec. 4.1).

- the G16 grism available at EFOSC2@NTT covers the range 6015–10320 Å and, according to the ESO web page[3], spectra are affected by second order contamination at wavelengths longer than 7170 Å (i.e., $\simeq 70\%$ of the wavelength range is contaminated).

- the R200 grism used with CAFOS@CAHA 2.2m covers the wavelength range 6300–11000 Å and according to the user guide manual[4] may be affected by second order contamination at the very edge only, beyond 10000 Å.

- the grism 5 available at BFOSC@1.5m Cassini covers the 4800–9800 Å range and according to the instrument manual[5] it is not contaminated by the second order spectrum.

[2] http://www.tng.iac.es/instruments/lrs/
[3] http://www.eso.org/sci/facilities/lasilla/instruments/efosc/inst/Efosc2Grisms.html
[4] http://w3.caha.es/alises/cafos/cafos22.html
[5] http://www.bo.astro.it/~loiano/TechPage/pagine/BfoscManualTechPage/BfoscManual.htm

1.1.1 Second order contamination correction

We discuss in this section the strategy adopted for the second order contamination correction. A detailed description of the procedure used for each instrument is presented in the corresponding section.

We adapted the method described by Sánchez-Blázquez et al. (2006) to correct the spectra for second order contamination.
This method requires the observed spectra of a blue and a red star and their flux calibrated spectra (from a database or other sources, without second order contamination).
These data are used to compute the response curves C_1 and C_2 for the light issuing from the first and second order respectively which, in turn, are used to flux calibrate and remove the second order contamination from any observed spectra (no matter the colour of the star).

Spectra are first reduced according to the standard recipe, subtracting bias and overscan if available, and correcting them for flatfield. The details of the spectra extraction and wavelength calibration are described in a separate document on the spectroscopic reduction (GCC-001).

If we label *b* the blue star and *r* the red star, we can label S_b and S_r their extracted, wavelength calibrated spectra, that can be expressed as:

$$S_b = C_1 T_b + C_2 T_{2b} \qquad S_r = C_1 T_r + C_2 T_{2r} \tag{3}$$

where T_b and T_r are the tabulated data (true flux calibrated spectra from literature[6]) for b and r, respectively, and T_{2b} and T_{2r} are T_b and T_r re-sampled and shifted to the second-order wavelength range (assuming that the mapping function is known). C_1 and C_2 represent the instrumental response for the light issuing from the first and second dispersion orders, respectively. Solving the system of equations, we obtain the response curves as

$$C_2 = \frac{T_b S_r - T_r S_b}{T_{2r} T_b - T_{2b} T_r} \tag{4}$$

and

$$C_1 = \frac{S_b - C_2 T_{2b}}{T_b} \tag{5}$$

Once the response curves C_1 and C_2 are known, the flux calibrated spectrum blueward of the second order contamination (i.e from 3350 to 6700 Å in Sánchez-Blázquez et al. 2006) can be

[6]Before doing any operation, we correct the literature spectra for the heliocentric velocity. In this way we add to the literature spectrum the same radial velocity of the observed star, due to the motion of the observer in the direction of the star. We use the IRAF tasks *rvcorrect* to compute the heliocentric velocity and *dopcor* to apply it. To be noted that the velocity value given by *rvcorrect* must be used with the opposite sign in *dopcor* to correct the observed spectrum or with the same sign to move the literature spectrum on to the observed spectrum. Due to the small relative velocities expected for our targets, of the order of a few tens of kilometres per seconds, we expect shifts not larger than $\simeq$ 1Å, hence the correction is practically negligible. Nevertheless, because it is a systematic effect, we take it into account.

obtained as:

$$S'_b(\lambda < 6700) = \frac{S_b}{C_1} \tag{6}$$

After re-sampling and shifting S'_b by the proper amount (6700 Å in Sánchez-Blázquez et al. 2006) (the resulting spectrum of these operations is called S'_{2b}), we finally obtain the whole calibrated spectrum as

$$S'_b = \frac{S_b - C_2 S'_{2b}}{C_1} \tag{7}$$

The second order correction method described above can not be directly applied to our data for two reasons:

1. the original method is used to correct observed spectra that cover the whole range of interest ($\simeq 3300 - 7500$ Å) in a single image. In our case we usually have two different setups (a blue and a red grism) that cover the whole optical range, this also implies that the blue and red spectrum of the same star may be at different airmasses;
2. in the original method, the equation of the dispersing element (a grating) is known ($\lambda_{1st\ order} = 2 \times \lambda_{2nd\ order}$), while the equation of the grism used in our observations is not known *a priori*.

In order to apply the same method to our data we proceed as follows:

- we join the blue and red spectra of the same star in a single spectrum. We join them at an arbitrarily wavelength, but shorter than the wavelength where the second order contamination is expected to start. The fact that the counts of the blue and red sides do not match, as shown in Fig. 2, is not important for the procedure. Nevertheless the two spectra must be scaled at the same airmass to be joined. Here is a subtle point: the blue spectrum should be corrected for extinction to match the airmass of the red spectrum. Correcting for extinction the red spectrum to the blue airmass or correcting both for extinction to bring them above the atmosphere would introduce errors because the blue light contaminating the red spectrum would not be properly corrected for extinction when applying a standard extinction curve[7]. These two spectra represent S_b and S_r.
- When possible, we derive the grism dispersion law analyzing the blue and red spectra of the same star. The absorptions lines in the blue spectrum may in fact be visible in the red spectrum too, especially if first and second order spectra are relatively well separated, as shown in Fig. 1. In this case, the comparison between the

[7]The extinction in the blue is much higher than in the red, so when we correct for extinction a red spectrum, its blue contamination will be undercorrected.

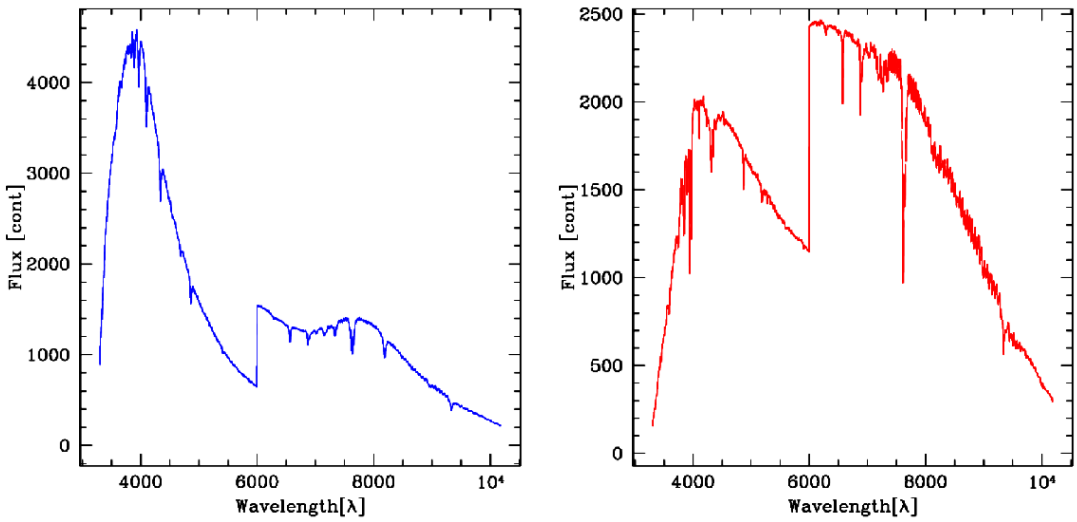

FIGURE 2: Composite observed spectra (Gr#11+Gr#16 EFOSC2, joined at 6000 Å) of Feige110 (our blue star, left panel) and LTT1020 (our red star, right panel). The red portion of both spectra is affected by second order contamination, which is much more evident in the blue star spectrum, where a "bump" is clearly visible in the 7000-8500 Å wavelength range.

features of the second order spectrum and the features of the first order spectrum allows us to determine the function that maps the first order into the second order.

With these ingredients it is possible to compute the response curves C_2 and C_1. The method described by Sánchez-Blázquez et al. (2006) can then be adapted to our data with some important *caveats*:

- because the full wavelength range is not covered with simultaneous images, non-photometric conditions can affect the red and the blue spectra and change the "shape" of the combined observed spectrum. This means that C_1 and C_2 can have wrong shapes and zero points;
- Once C_1 and C_2 have been correctly derived, the blue and red spectra acquired under not photometric but grey conditions[8] may have wrong relative flux, thus affecting their correction even if C_1 and C_2 are correct.
- The correct shape and relative flux of blue and red spectra acquired under not photometric and not grey conditions can not be recovered.

Possible solutions are:

[8]The extinction produced by veils or thin clouds is expected not to alter significantly the spectral shape (Oke 1990, Pakštiene & Solheim 2003).

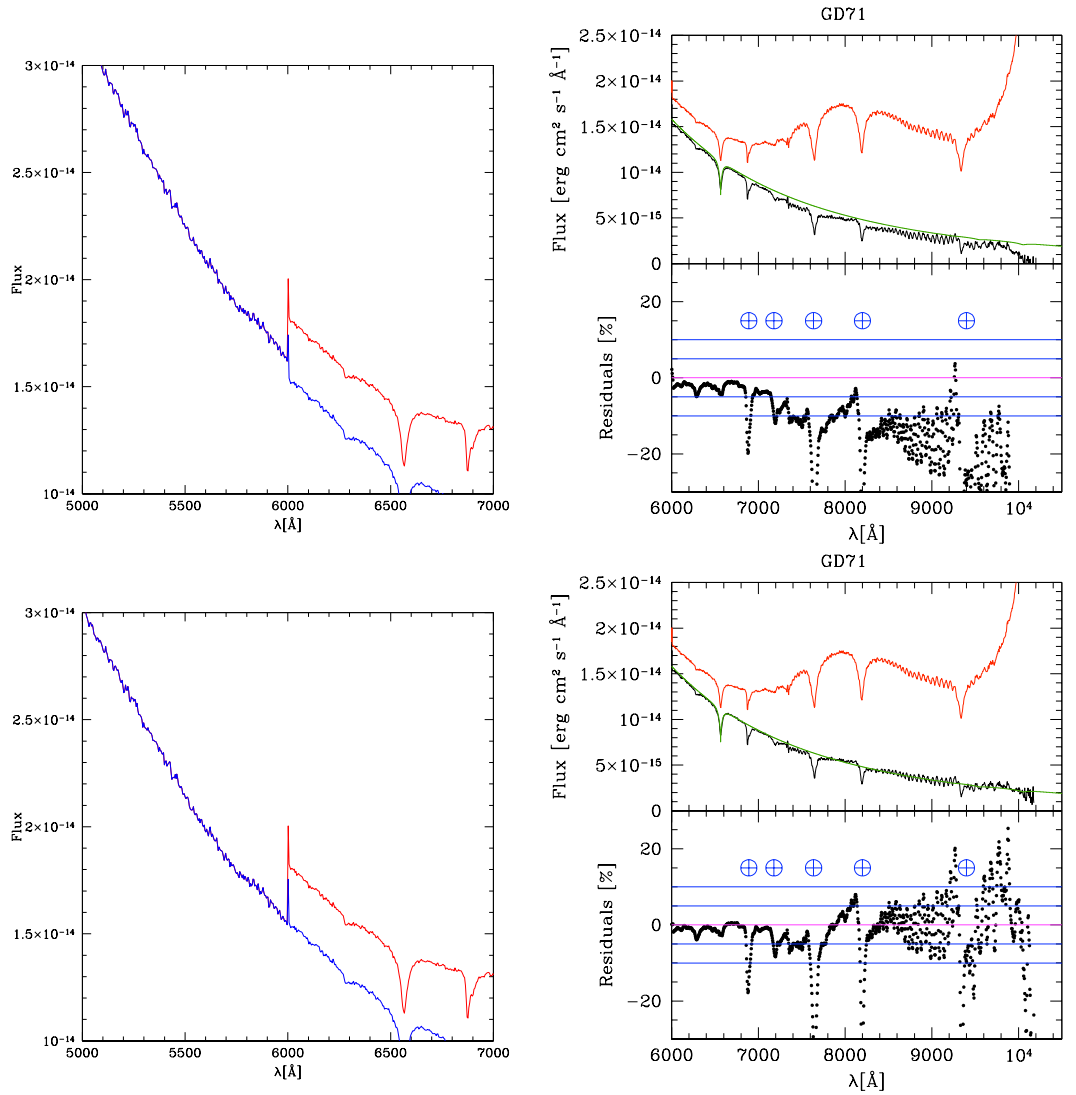

FIGURE 3: Left panels: GD71 flux calibrated spectrum (red line: contaminated Gr#16 spectrum; blue line: Gr#11+Gr#16 spectra, joined at 6000 Å after correction of the second order contamination). Right panels: second order contaminated spectrum (red line), corrected spectrum (black line), CALSPEC spectrum (green line). Residuals of the corrected spectrum with respect to the CALSPEC one are shown (telluric features are indicated). In the upper panels no correction has been applied to the exposure times and the left panel shows a small mismatch between the blue and the red second order corrected spectrum. In the lower panels the exposure time of the Gr#11 spectrum has been scaled to match the red spectrum after the second order correction (in this example the corrected red spectrum was fainter than expected, probably because of veils, hence over-corrected by the second order contamination correction). The correction is performed again with the new exposure times to obtain the final result (right panel). The scaling produce significant smaller residuals.

- compute C_1 and C_2 with data obtained under photometric conditions only;

- check the absolute calibration of each blue and red spectrum while applying the second order correction: the blue and red spectra acquired under non photometric but grey conditions may need to be scaled to match and reproduce the correct relative flux, see Fig. 3. In this case, while the shape of the spectrum can be recovered, the zero point is not reliable any more and it must be set by comparing synthetic and absolute photometry or using a spectrum of the same star observed in photometric conditions to set the proper zero-point.
- Spectra acquired under not photometric (and non grey conditions) can not be properly corrected for second order.

In Sec. 3.1 and 4.1 we apply this procedure to real data obtained with EFOSC2 at NTT and DOLoRes at TNG respectively. The C_1 and C_2 curves computed for these instruments can be used to correct spectra obtained with our instrumental setup.

To be noted that the second order corrected spectrum given by equation 7 is also flux calibrated. Nevertheless, because of C_1 and C_2 are not computed for each night, we suggest to produce second order corrected spectra in ADU by equation 8

$$S'_b = S_b - C_2 S'_{2b} \tag{8}$$

and then to proceed as usual computing the response curve for absolute flux calibration night by night. More details on the second order correction application can be found in GA-006.

1.2 Instrumental polarization

Both curved and plane mirrors are known to change to some degree the polarization properties of the incoming light. Their reflectivity may be different for different directions of linear polarization, in a wavelength dependent way (see Breckinridge & Oppenheimer 2004 and references therein). An incoming beam of non-polarized light will be polarized according to this difference of efficiency. This might affect the sensitivity of the whole observing system if the light beam encounters other polarization-sensitive optical elements after reflection. The degree of induced polarization depends on the angle of incidence: the maximum degree of (linear) polarization occurs for an incidence angle which depends on the material, called *polarization angle*. Refractive dispersing elements (grisms, in our case) may also produce some degree of polarization, in principle, and/or have different transmission efficiencies for different polarizations of the incoming light.
Another important aspect to be considered arises from the possibility that the incoming star light is *intrinsically* polarized. In such a case, the reflection/transmission of the light beam by a mirror and/or a combination of mirrors and dispersing elements may, in principle, introduce selective light losses. Any polarization induced by the reflection may also produce similar losses in the interaction with other polarization-sensitive optical elements. This seems particularly likely to produce subtle unwanted effects when the reflecting/dispersing elements are rotated

in the plane perpendicular to the light path in different ways depending on the telescope pointing. For instance, derotators mounted before spectrographs at Nasmyth foci (a very common configuration in modern telescopes) change the relative position angles between the flat mirror deviating the main light path to the lateral focus and any reflecting/dispersing optical element of the spectrograph. This may lead, for example, to differential efficiency on waves of a given direction of polarization by a grism fed by a flat mirror, to a degree that is dependent on the relative position angles of the elements, that may be different at any pointing. Even if the effect were completely wavelength independent, different pointings would lead to different orientations of potentially polarizing optical elements in the plane perpendicular to the beam. The net result would be that the sensitivity of the whole instrumental set-up would depend on the pointing, that is obviously not the same even for the same star observed at different times.

We can envisage three cases that are exemplified by three different instruments that we used during our campaigns:

1. The light beam encounters just one optical element potentially sensitive to polarization, which is the dispersing element (grism) as in the case of CAFOS@CAHA. If the incoming light is non-polarized, there is no effect on spectrophotometry. If the incoming light is polarized, there may be a difference in the response depending on the actual orientation of the grism in the plane perpendicular to the direction of the light beam. This orientation may change at any pointing according to the parallactic angle.

2. There is more than one element potentially sensitive to polarization, but their relative orientation in the planes perpendicular to the direction of the incoming beam are fixed, as is the case of the flat mirror feeding the grisms of BFOSC@Cassini. The net result is the same as for the first case above[9].

3. There is more than one element potentially sensitive to polarization, and their relative orientation in the planes perpendicular to the direction of the incoming beam changes, depending on the telescope pointing. This is the case of the flat M3 mirror of TNG and NTT that drives the main light path to the Nasmyth focus where it feeds the grism of the DOLoRes and EFOSC2 spectrographs, mounted on the derotator device. In this case some polarization effect can be induced even on non-polarized incoming light, and the grism may respond slightly differently – in terms of efficiency – to differently polarized light (resulting in a light loss depending on the relative orientation of the two elements).

Most of our candidate SPSS are relatively bright, nearby and not much extincted white dwarfs

[9]It is interesting to note that in the web site: (`http://www.ls.eso.org/sci/facilities/lasilla/instruments/efosc-3p6/`) of a very similar instrument (EFOSC2) it is reported, : "Preliminary analysis of instrument polarization shows $< 0.1\%$ at field centre, and $\sim 0.4\%$ at the edge (07/07/2005)". This provides a rough quantitative idea of the polarization that must affect BFOSC, as well.

TABLE 2: Telescopes/Instruments used in the spectroscopic observations of the Gaia SPSS

Telescope	Instrument	Location	Ref.
Cassini 1.5m	BFOSC	Loiano, Italy	Sec. 2
ESO NTT	EFOSC2	La Silla, Chile	Sec. 3
TNG	DOLoRes	Roque de los Muchachos, Spain	Sec. 4
CAHA 2.2m	CAFOS	Calar Alto, Spain	Sec. 5

and hot stars. The maximum degree of linear polarization that we can expect in the worst cases is much less than 5%. For typical high efficiency optical elements in the observational set-ups of the type 1 and 2, above, it is very unlikely that polarization can affect the accuracy of spectrophotometry at more than $\sim 1\%$ level[10].

In the following sections we examine in more detail the performances of the spectrographs used in our observing campaign and listed in Table 2. A summary of the results can be found in Sec. 6.

2 BFOSC@Cassini 1.5m

2.1 BFOSC second order

Two grisms are used with BFOSC: grism 3, covering the 3300–6420 Å range, and grism 5, covering the 4800–9800 Å range. According to the instrument manual[11], none of them is affected by second order contamination and in any case the red end of the grism 3 spectrum can be recovered, if necessary, from the grism 5 spectrum. A blue star (GD71) spectrum taken for the purpose at high airmass ($\simeq 2$) with grism 5 and a 2" slit was examined to look for the presence of a possibly separated second order spectrum. No hint of appreciable second order spectrum was detected (see Fig. 4)

2.2 BFOSC polarization

Due to the optical telescope configuration, no significant polarization is expected (see Sec. 1.2).

[10]While potentially highly polarized sources should be avoided as candidate SPSS (as for instance DP white dwarfs or heavily extincted stars) we stress that there is no observational strategy that can completely avoid the problem.

[11]`http://www.bo.astro.it/~loiano/TechPage/pagine/BfoscManualTechPage/BfoscManual.htm`

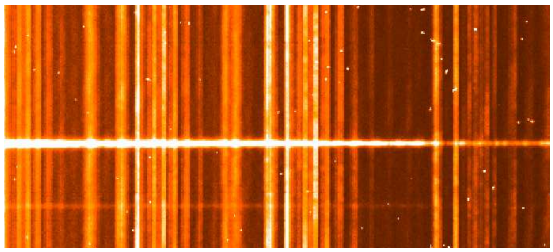

FIGURE 4: Detail of a Gr#5 slit 2" spectrum of GD71 observed at airmass 2.04 with parallactic angle. Wavelength increases towards the right, where despite of the high airmass, no second order spectrum is visible.

2.3 BFOSC Conclusions

No second order contamination is expected to affect the data obtained with the instrumental setup used in our observing campaign (grism 3 and grism 5). Due to the optical telescope configuration, polarization is not expected to be an issue.

3 EFOSC2@NTT

3.1 EFOSC2 second order

The EFOSC2@NTT grism 16 covers the range 6015–10320 Å and, according to the ESO web page, spectra are affected by 2^{nd} order contamination at wavelengths longer than 7170 Å (i.e., $\simeq 70\%$ of the wavelength range is contaminated).

To verify and quantify the effect, spectra of a blue and a red star, namely Feige110 ($V = 11.832$, $B - V = -0.305$, Landolt & Uomoto 2007), and LTT1020 ($V = 11.510$, $B - V = 0.551$, Landolt 1992) were acquired with EFOSC2 (LORAL CCD#40). The corresponding literature data that we used were: fltt1020.dat[12] (Hamuy et al., 1992, 1994) and feige110_stisnic_003.ascii (CALSPEC[13] and references therein). Each star was observed with Gr#11 (3380–7520 Å) and Gr#16 (6015–10320 Å) through a 10" slit to minimize flux losses, and with the 1.5" slit to obtain a better wavelength calibration (as explained in GCC-001).

Data reduction was performed as described in GCC-001. We note that Gr#16 spectroscopic flat fields were acquired soon after each target, as suggested in the EFOSC2 manual (Section 3.5.7)[14], to better remove fringing and we note also that the overscan strip is inadequate for bias

[12] ftp://ftp.eso.org/pub/stecf/standards/ctiostan/
[13] http://www.stsci.edu/hst/observatory/cdbs/calspec.html
[14] http://www.eso.org/sci/facilities/lasilla/instruments/efosc/doc/manual/EFOSC2manual_v4.0.pdf

subtraction[15].

In order to apply the method described in Sec. 1.1.1 to our data, we proceeded as follows:

- we joined the Gr#11 and Gr#16 spectra of the same star in a single spectrum. We arbitrarily joined them at 6000 Å i.e., before the second order contamination is expected to start, as shown in Fig. 2 and described in Sec. 1.1.1.
- We derived the dispersion law from the blue and red spectra of LTT1020. The absorptions lines in the blue spectrum are in fact visible in the red spectrum as well (see Fig. 1). The comparison of the features of the second order spectrum extracted from the Gr#16 image with the blue Gr#11 spectrum of the same star, allowed us to determine the function that maps the first order wavelength onto the second order (see Fig. 5 and Tab. 3).

In all these tests, the initial extinction correction was based on the CTIO extinction curve taken from IRAF[16] (onedstds$ctioextinct.dat), but then we computed the extinction curve with our own data, using spectra of LTT1020 observed at different airmasses on 30 Nov 2008. Fig. 6 shows the resulting extinction curve. The match between the ESO user manual 1993[17] extinction curve ad our own is very good up to 7400Å. The extinction curve at longer wavelengths is based on the Gr#16 spectra corrected for second order contamination. The resulting extinction values lies between the CTIO curve and the one provided by the ESO user manual, that stops at 9000Å. The oscillations visible above 7400Å are probably due to the manipulation operated on the Gr#16 spectra to remove the second order contamination and to the noise introduced by the fringing.

The second order correction does not change significantly when assuming a slightly different function mapping the first into the second order, that can be obtained repeating the measurement of the features shown in Tab. 3, or fitting the relation with a slightly different polynomial.

Fig. 7 shows a second order polynomial fit of our data (Tab. 3), which produces the following relation:

$$\lambda_{2^{nd}ord} = -3815 + 3.271\lambda_{1^{st}ord} - 0.0001167\lambda^2_{1^{st}ord} \quad (9)$$

with a residual of $\sigma = 2.9$ Å (a first order polynomial fit gives a much larger residual of $\sigma = 13.01$ Å). The "true" flux calibrated spectra T_b and T_r have been taken from the literature

[15] http://www.eso.org/sci/facilities/lasilla/instruments/efosc/inst/Ccd40.html#summary

[16] IRAF is the Image Reduction and Analysis Facility, a general purpose software system for the reduction and analysis of astronomical data. IRAF is written and supported by the IRAF programming group at the National Optical Astronomy Observatories (NOAO) in Tucson, Arizona. NOAO is operated by the Association of Universities for Research in Astronomy (AURA), Inc. under cooperative agreement with the National Science Foundation.

[17] http://www.ls.eso.org/lasilla/Telescopes/2p2/D1p5M/misc/Extinction.html

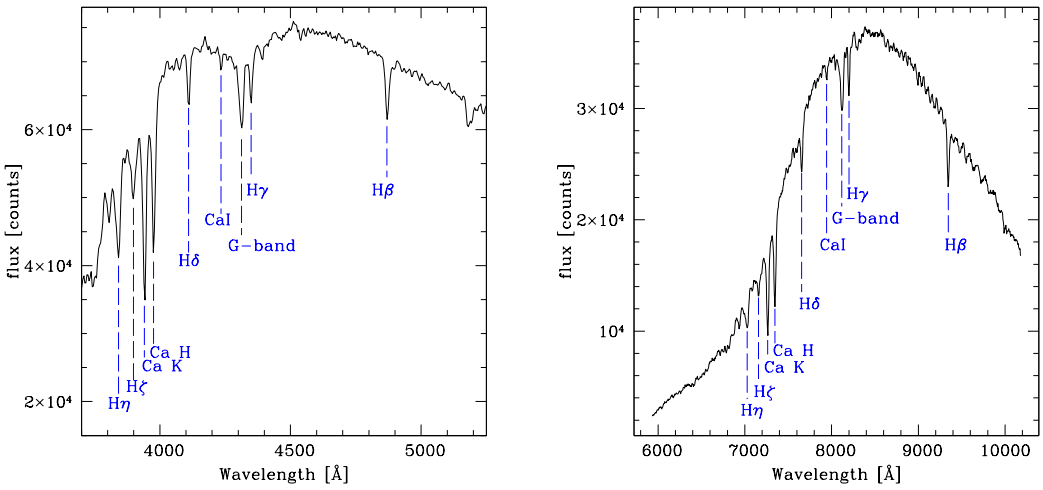

FIGURE 5: Left panel: detail of a Gr#11, observed spectrum of LTT1020; right panel: second order spectrum extracted from a Gr#16 spectrum of LTT1020 observed at high airmass (AM=1.92). Neglecting the overall shape, that is obviously different, it is possible to recognize the absorption lines pattern of the blue wavelength range in the red wavelength range.

TABLE 3: Position of the absorption lines shown in Fig. 5 in the 1^{st} order, Gr#11 and in the 2^{nd} order, Gr#16 spectra.

Line	1^{st} order, Gr#11 [Å]	2^{nd} order, Gr#16 [Å]
H_η	3841.55	7027.03
H_ζ	3898.82	7157.89
CaK	3940.88	7264.50
CaH	3975.36	7347.56
H_δ	4109.43	7655.65
CaI	4233.65	7942.25
$G-band$	4312.13	8118.39
H_γ	4349.64	8200.15
H_β	4869.50	9344.98

(CALSPEC and Hamuy et al. 1992, 1994, see Fig. 8). Fig. 9 shows the derived response curves C_2 and C_1 computed according to eq. 4 and eq. 5 and the percentage P of the first order spectrum falling in the second order spectrum, where $P = C_2'/C_1$, with C_2' representing C_2

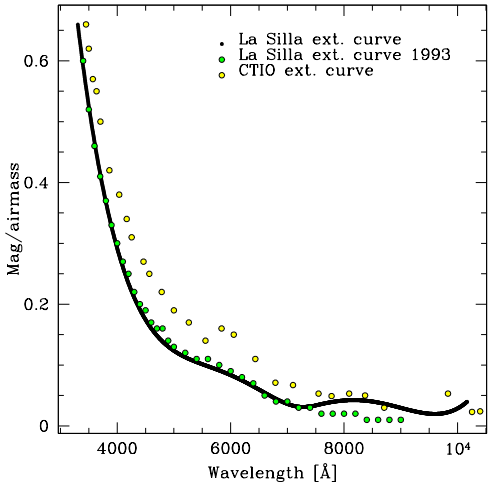

FIGURE 6: The extinction curve computed for La Silla (in black) is compared with the CTIO extinction curve and with the ESO user manual 1993.

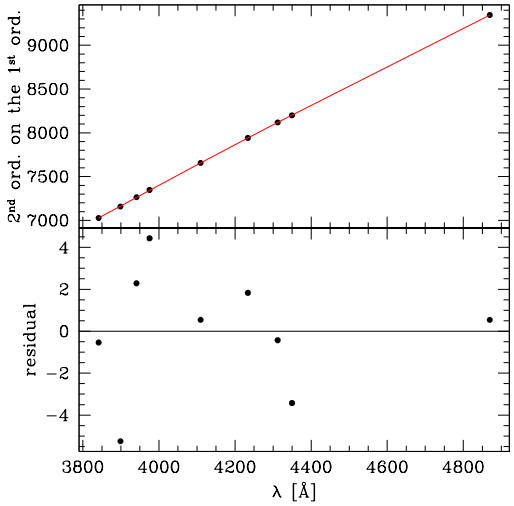

FIGURE 7: Second order polynomial fit of the relation between the first and second spectral orders of EFOSC2@NTT

shifted and re-sampled on the same wavelength range of C_1. P has been computed for two different epochs (2008/11/30 and 2011/08/29) and appears stable within $\sim 1\%$ with respect to the average curve, that is the actual curve we used for the second order correction. C_2 shows that the second order contamination starts well before 7170 Å, and indeed it seems to affect the whole Gr#16 spectrum. Fig. 3 (bottom-right panel) shows the red edge of the flux calibrated spectrum of an independent star (GD71, $V = 13.032$, $B - V = -0.252$, Bohlin et al. 1995, not used to compute C_1 and C_2) with and without second order correction, compared to the CALSPEC spectrum (gd71_mod_007.ascii). GD71 is a blue star that shows a clear second order contamination, that is pretty well corrected with the C_1 and C_2 response curves.

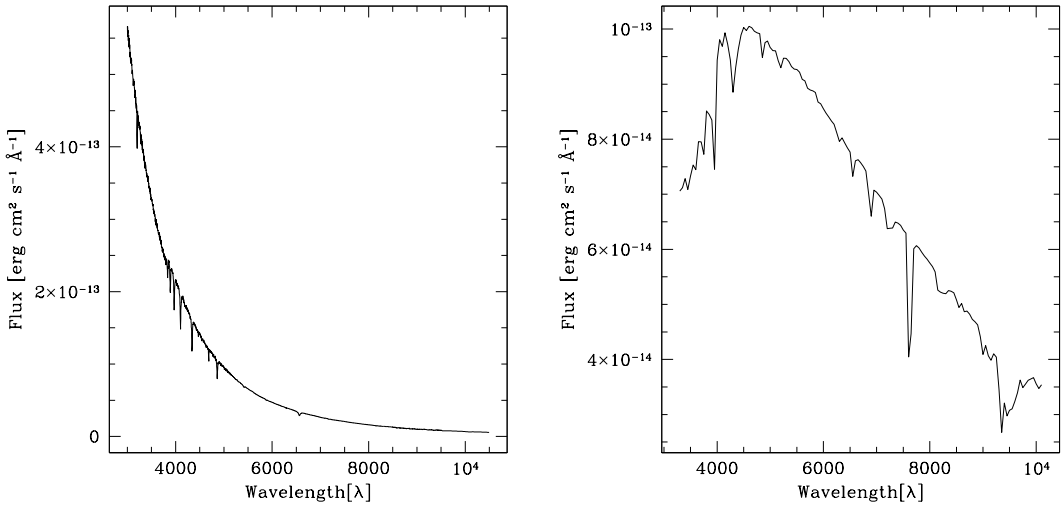

FIGURE 8: True flux calibrated spectra (not affected by second order contamination) of Feige110 from CALSPEC (feige110_stisnic_003.ascii, left panel) and LTT1020 from Hamuy et al. 1992, 1994 (right panel).

3.2 EFOSC2 polarization

Since EFOSC2 was moved to the Nasmyth focus of the NTT, a significant instrumental polarization related to the telescope pointing is expected (as discussed in Sec. 1.2). The ESO staff is working to characterize this effect[18]. We expect such effect to limit the accuracy of polarization measurement of polarized stars and to be less relevant for normal spectroscopic observations of unpolarized stars, which is our case. A more detailed study of the problem is presented for DOLoRes@TNG in Sec. 4.2, that is very similar.

3.3 EFOSC2 Conclusions

The second order contamination seems to start from the very beginning of the Gr#16 spectrum, i.e., at $\simeq$ 6000 Å, and covers all the spectral range following the relation shown in eq: 9. The C1, C2 curves and the percentage of the first order spectrum falling in the second one can be found in Wiki-Bo[19].

The conclusions for the polarization effect are the same reported for DOLoRes@TNG, see section 4.3.

[18] http://www.eso.org/sci/facilities/lasilla/instruments/efosc/inst/Efosc2PolarElements.html

[19] http://yoda.bo.astro.it/wiki/index.php/Spectroscopy_Reduction_and_Analysis

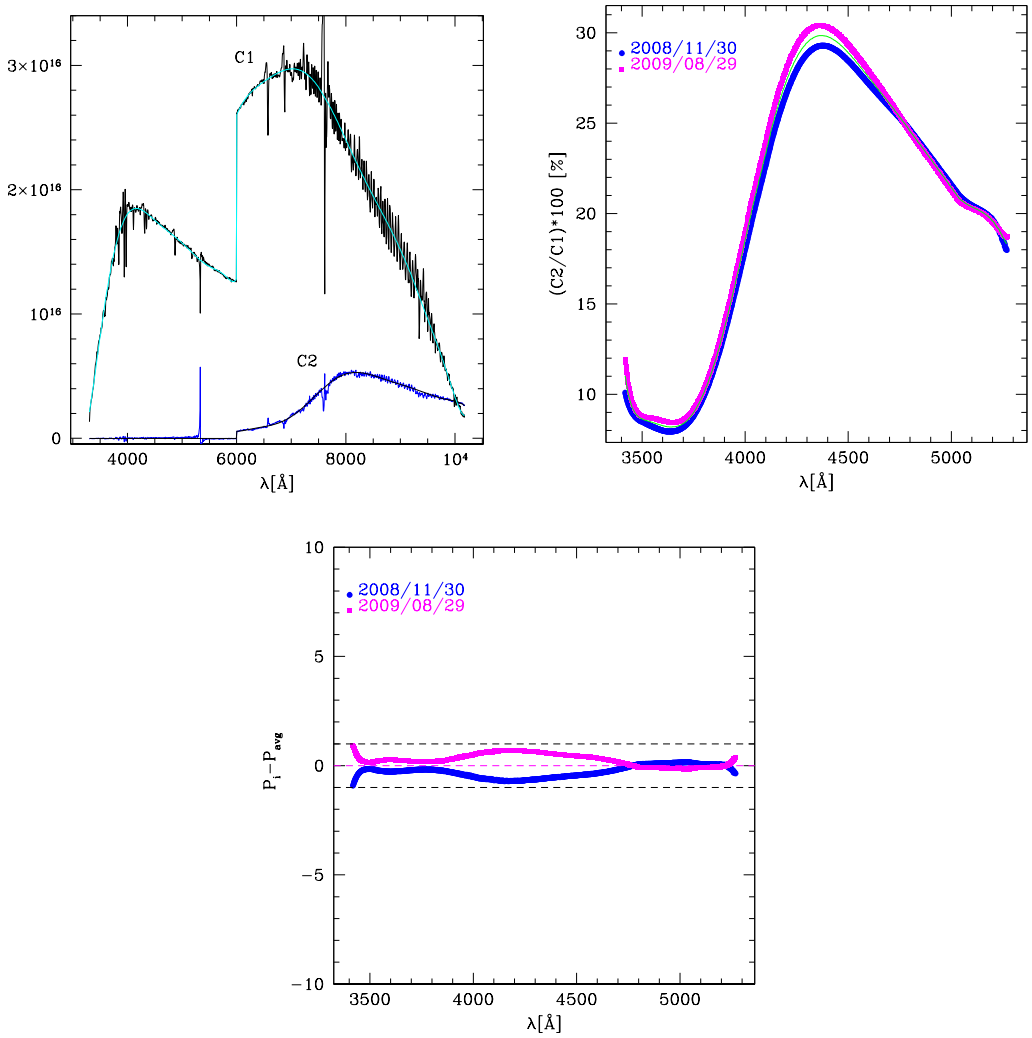

FIGURE 9: Top Left panel: C_1 (cyan) and C_2 (blue) response curves (based on data taken on 2008/11/30). The 6000 Å discontinuity is the effect of the merging of the Gr#11 and Gr#16 spectra, that are characterized by different zero points and response curves. C_1 and C_2 were fitted with a polynomial to obtain smooth curves. Top Right panel: percentage $P_i = C_2'/C_1$ of the first order (flux calibrated) spectrum falling in the second order spectrum (the results are based on data taken on 2008/11/30 and 2011/08/29, the green line shows the average of the two epochs) The third image shows the difference $P_i - P_{avg}$ where P_i is computed for the 2 epochs i and P_{avg} is the average curve. The maximum difference between the two curves is reached around 4200 Å and it amounts to less than 2%.

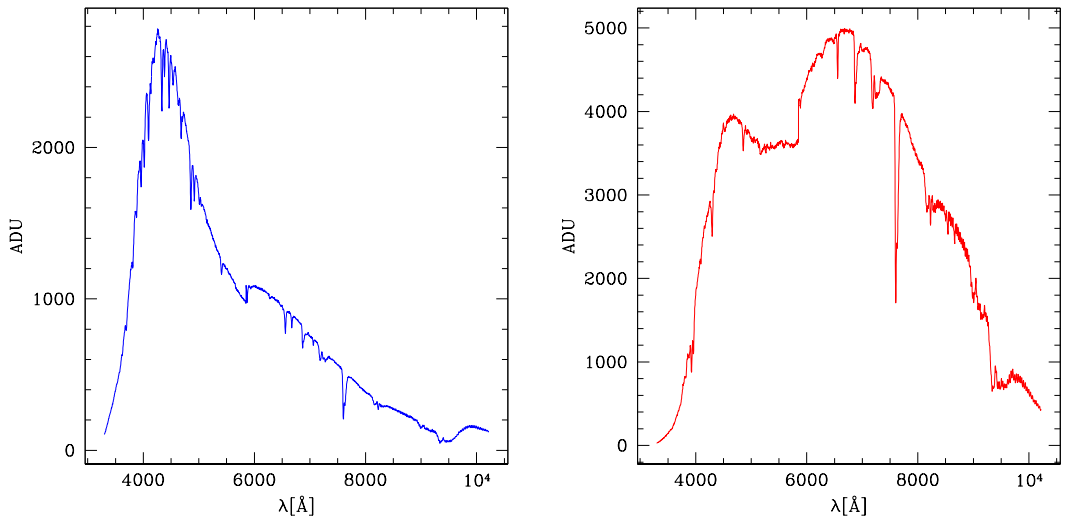

FIGURE 10: Composite observed spectra (LR-B + LR-R @DOLoRes) of HZ44 (left panel) and G146-76 (right panel). The jump at 5850 Å is where the two spectra were joined and is caused by the fact that spectra are in ADU and not absolutely flux calibrated.

4 DOLoRes@TNG

4.1 DOLoRes second order

The DOLORES LR-R grism has a built-in order-blocking filter cutting blueward of $\simeq 5000$ Å; nevertheless, spectra are affected by second order contamination, that can be noticed in blue stars spectra, starting around 9500 Å, see Fig. 10.

To quantify the contamination, spectra of a blue and a red star, namely HZ44 ($V = 11.673$, $B - V = -0.291$, Landolt & Uomoto 2007) and G146-76 ($V = 10.47$, $B - V = 0.68$, Høg et al. 2000), were acquired with DOLORES@TNG; GD153 ($V = 13.346$, $B - V = -0.281$, Bohlin et al. 1995), was observed, as well, to test the correction with an independent star.
In particular, each star was observed with LR-B/LR-R and the 5" slit to avoid flux losses, and with the 2" slit to obtain a better wavelength calibration (see GCC-001).
To have an additional spectrum free from contamination (besides the CALSPEC one), we also acquired LR-R spectra of the same stars, using the I filter to block any light from the second order. All these spectra provide full comparison spectrum of each star, free of second order contamination.

All spectra were reduced with the procedures described in GCC-001. Similarly to what done in Sec. 1.1.1, we arbitrarily joined the blue and red spectra at 5850 Å. The resulting spectra (S_b and S_r in our equation 3) are shown in Fig. 10. We were forced to use equation 1, which is valid for gratings, even if we are using grisms, because there were too few lines belonging to both

orders[20] to reconstruct the second order dispersion law (see Sec. 3.1). The "true" flux calibrated spectra T_b and T_r are the flux calibrated spectra obtained from the literature, if available, or by combining the LR-B, LR-R and LR-R+I filter spectra, calibrated with the sensitivity curves corresponding to each setup. Then we computed the response curves C_2 and C_1 according to eq. 4 and eq. 5, that are shown in Fig. 11, together with the percentage P of the first order spectrum falling on the second order spectrum, where $P = C_2'/C_1$, with C_2' representing C_2 shifted and resampled on the same wavelength range of C_1. The derived curves and contamination percentages were compared with those obtained observing different stars, namely GD153 (DA1 Bohlin et al. 2005, V=13.346 Bohlin et al. 1995) and KF06T2 (K1.5III Reach et al. 2005, V=13.83[21] Lasker et al. 2008), in a different night. The results are rather similar (see Fig. 11), differing less than 1% in the worst spectral region. The 5850 Å discontinuity is the effect of the merging of the LR-B and LR-R spectra, that are characterized by different zero points and response curves. C_1 and C_2 can be fitted with a low order polynomial to obtain a smoother trend.

The second order contamination starts at $\simeq$ 9450 Å, where C_2 shows a significant deviation from zero (the exact starting point is not clearly visible in the spectra because a strong H_2O telluric absorption affects the region between 9000 and 10000 Å). Fig. 12 shows the second order contamination on the observed spectra of a blue (HZ44) and red (G146-76) star. As expected, the contamination is more evident for the blue star (having a larger contaminating flux) than for the red one.
Fig. 13 (left panel) shows the flux calibrated spectrum of an independent star (GD153, not used to compute C_1 and C_2) with and without second order correction, compared to the CALSPEC spectrum. GD153, a blue star, shows a clear second order contamination that is roughly corrected with the C_1 and C_2 response curves. We note that the correction is based on the assumption $\lambda_{1st\ order} = a \times \lambda_{2nd\ order} + b$, with $a = 2$ and $b = 0$, that is an approximation of the unknown grism dispersion law. The assumption is consistent with $a = 2.027$ and $b = 0$ that have been computed as it follows. We analyzed He, Ne, Ar wavelength calibration lamp spectra taken separately with LR-R and the 2" slit. The He arc was taken through the B filter with 1h exposure time, and one of the 3 lines visible is at the red edge of the spectrum, where no helium lines are expected to be (see Fig.14). These lines were wavelength calibrated using the NeAr calibration arcs. The two lines in the blue are at 5013.27 Å and 5871.8 Å, while the *red* line is at 9553.3 Å. The first two lines are most probably the helium emission lines at 5015.7 and 5875.6 (the small offset can be due to wavelength calibration errors and/or shift introduced by the B filter in the He spectrum). If we assume that the second order spectrum is roughly shifted by a factor two with respect to the first order (as in a grating), the 9553.3 should correspond to a line around 4777 Å. If we look for He lines around this region we find the 4471.5, 4713.1 and 4921.9 Å lines. The most reasonable coincidence seems to be the 4713.1 line. With one point only we can not make any fit but a simple ratio 9553.3/4713.1=2.027. Fig. 13 shows that the

[20] We tried to infer the dispersion law by observing a blue arc with LR-R+U,B,V filter to suppress the first order red spectrum and to identify the second order blue emission lines. Because the built-in second order-blocking filter could not be removed, the net result was an almost empty image, with one or two faint lines. Also a spectrum taken for purpose at high airmass could not be used to separate the two spectra as in the case of Fig. 1.

[21] Photographic band (green).

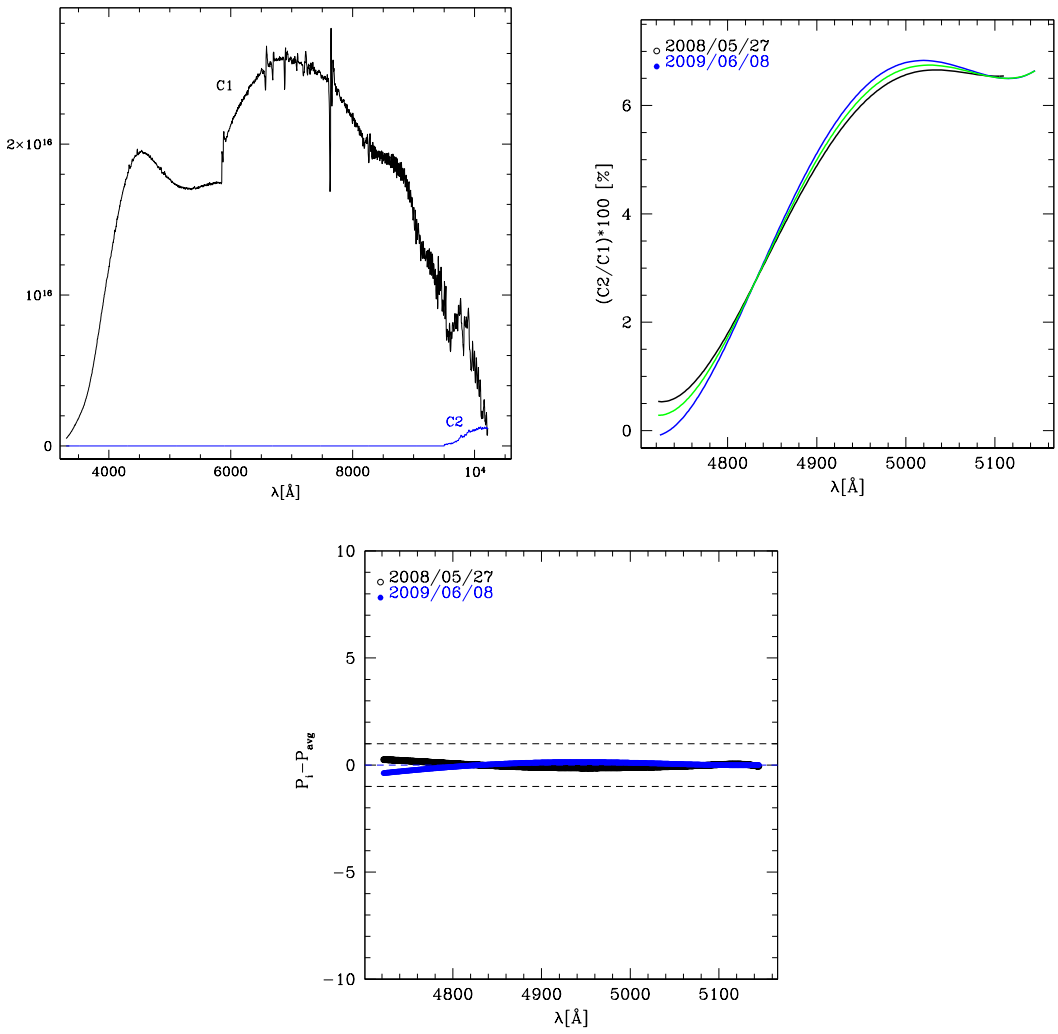

FIGURE 11: Top Left: C_1 (in black) and C_2 (in blue) response curves (based on data taken on 2008/05/27). Top Right: percentage P_i, computed for two different epochs i, of the first order (flux calibrated) spectrum falling in the second order spectrum. The black and blue curves are polynomial fit (to obtain a smooth trend) of the data acquired on 2008/05/27 and 2009/06/08. The green line, P_{fit}, shows the simultaneous fit of both the curves. The third image shows the difference $P_i - P_{fit}$.

second order correction obtained assuming $a = 2.027$ or $a = 2.0$ are very similar. Hence we assume that the second and first order are linked by the following relation:

$$\lambda_{2^{nd}ord} = 2.0 \times \lambda_{1^{st}ord} \tag{10}$$

Our guess is based on one line only, hence a linear relation $\lambda_{2^{nd}ord} = a \times \lambda_{1^{st}ord} + b$ with $b \neq 0$ can not be ruled out.

We also tried to derive the dispersion law of the second order spectrum by acquiring the spectrum of a blue star observed at high airmass in order to separate first and second order spectra

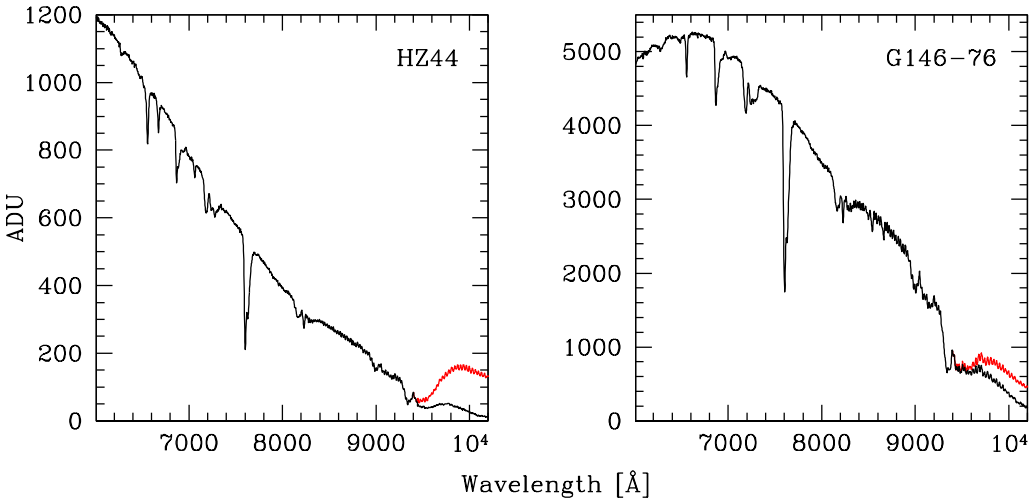

FIGURE 12: The LR-R grism shows second order contamination starting at $\simeq$ 9450 Å (see red lines). The response curves C1 and C2 are used to remove the second order contamination from any observed spectra (no matter the colour of the star): see the black lines

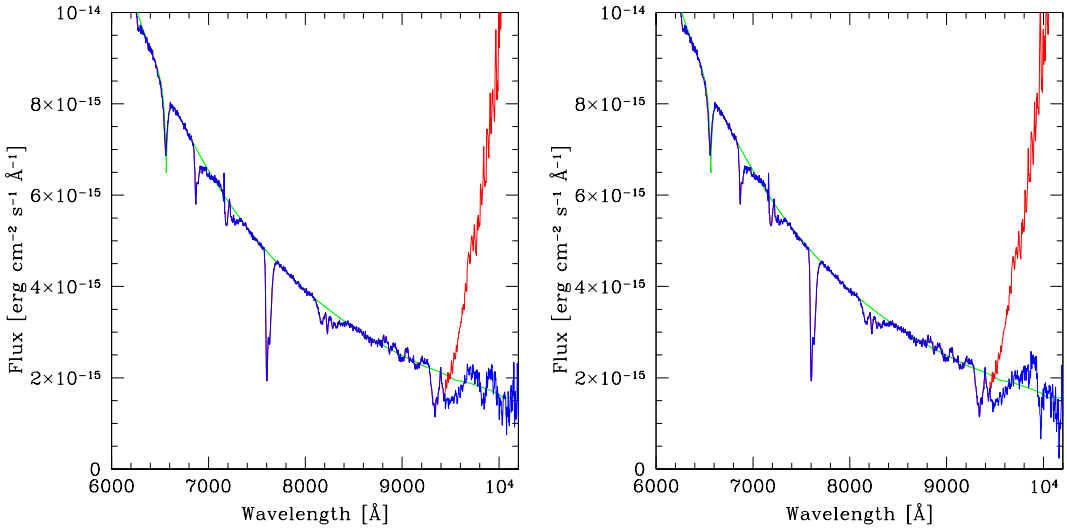

FIGURE 13: Red edge of GD153 spectrum. Red line: second order contamination, blue line: corrected spectrum, smooth green line: CALSPEC spectrum. Left panel: $\lambda_{1st\ order} = 2 \times \lambda_{2nd\ order}$, right panel $\lambda_{1st\ order} = 2.027 \times \lambda_{2nd\ order}$.

(see Fig. 15). Unfortunately the second order spectrum does not show any feature so it is not possible to find the exact relation that maps the first into the second order. Also the analysis of the wavelength calibration arcs (Ar+Kr+Ne+Hg) and of the skylines are not helpful because no clear blue emission line is visible where the second order is expected to contaminate the spectra and no emission line is well visible in the region 4700–5100 Å that is expected to originate the

contamination.

The DOLORES LR-B grism was not expected to be affected by second order contamination, nevertheless the analysis of the spectra acquired with it shows peculiarities that mimic or can be easily explained by second order contamination. These peculiarities were not evident in the spectra and hence they passed unnoticed until later stages of spectra reduction and analysis, while the LR-R second order contamination was obvious already in the uncalibrated extracted spectra, especially for the blue stars. The first hints of a possible LR-B contamination appeared in the response curves built by means of spectra of stars of different spectral type (Fig. 16). The response curves coincide pretty well in the blue, up to ~ 6000Å and then diverge.

To further investigate the effect, a response curve was built using the 2 hottest stars (BD+284211 and GD153). If the LR-B spectra are contaminated by second order light, we expect the response curve to include this effect with the result of cancelling it out when calibrating hot blue stars. On the other hand we expect cold stars, that are affected by a fainter second order contamination with respect to hot blue stars, to be "overcorrected" and hence to deviate from the expected shape. This is exactly what happens when calibrating hot and cold stars, as shown in Fig. 17, where late spectral types deviate more and more from the expected flux (given by the template or by the LR-R spectrum in the overlapping region).

The LR-B contamination also affects the extinction curve derived from the blue spectra. Fig. 18 shows the comparison of the King (1985) extinction curve for La Palma and the one derived using LR-B and LR-R spectra. If LR-B spectra are rejected above 6000Å, where the second order contamination seems to occur, the resulting extinction curve better follows the King (1985) curve and the "bump" in the 6000–8000Å range is less pronounced.

4.2 DOLoRes polarization

The TNG is a copy of the ESO NTT (see section 3.2). Owing to the Nasmyth optical system, at least a folding mirror is introduced in the optical path. Because the relative orientation of this mirror with respect to the sky varies with the telescope pointing, instrumental polarization is expected, see Giro et al. (2003).

FIGURE 14: LR-R spectrum of the He lamps observed trough the 2" slit + B filter and 3600 sec exposure time. Three lines are visible, two in the blue (left) and one unexpected in the red (right).

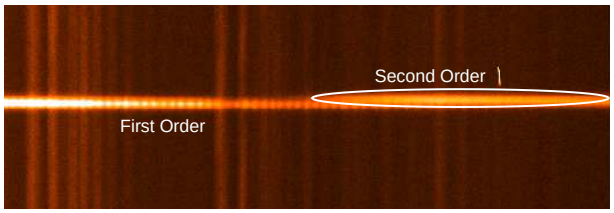

FIGURE 15: Red edge of Feige 110 spectrum obtained with DOLORES@TNG, grism LR-R and slit 2", at airmass 2.29 and with 90 sec exposure time. The second order contamination is clearly visible but it is not well separated from the first. (TNG staff courtesy)

The highly polarized star HD155197[22] was selected to emphasize possible flux modulation produced by instrumental internal polarization. HD155197 was spectroscopically observed at different position angles (0, 45, 90 and 135 degrees), with grisms LR-B and LR-R, through the 5" slit, to check the combined effect of the source polarization and the internal instrumental polarization at the Nasmyth focus and its dependency on wavelength. Narrow slit (2") spectra were taken with both grisms at the last position, i.e., 135 deg, and calibration lamps (He for LR-B, Ar for LR-R) were acquired with the same setup at this position.

[22] V=9.20, spectral type: A0, V band polarization: 4.38%±0.030, see Turnshek et al. (1990).

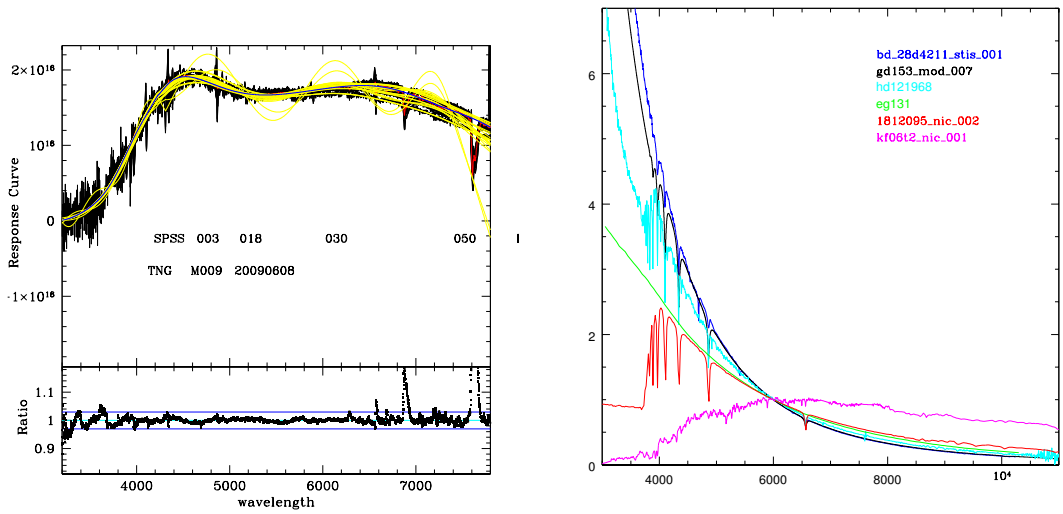

FIGURE 16: Left: upper panel: response curve (blue line) obtained fitting the median (red line) of the curves obtained using stars of different spectral types (black lines), namely SPSS018 (BD+284211 Op), SPSS003 (gd153 DA1), SPSS030 (hd121968 B1), SPSS050 (eg131 DBQ5), SPSS037 (1812095 A5), SPSS047 (KF06T2 K1). Yellow lines are not relevant fits. Lower panel: residual of the fit (blue line) of the median of the response curves with respect to the median (red curve). Right: normalized spectra of the 6 stars used to build the response curves.

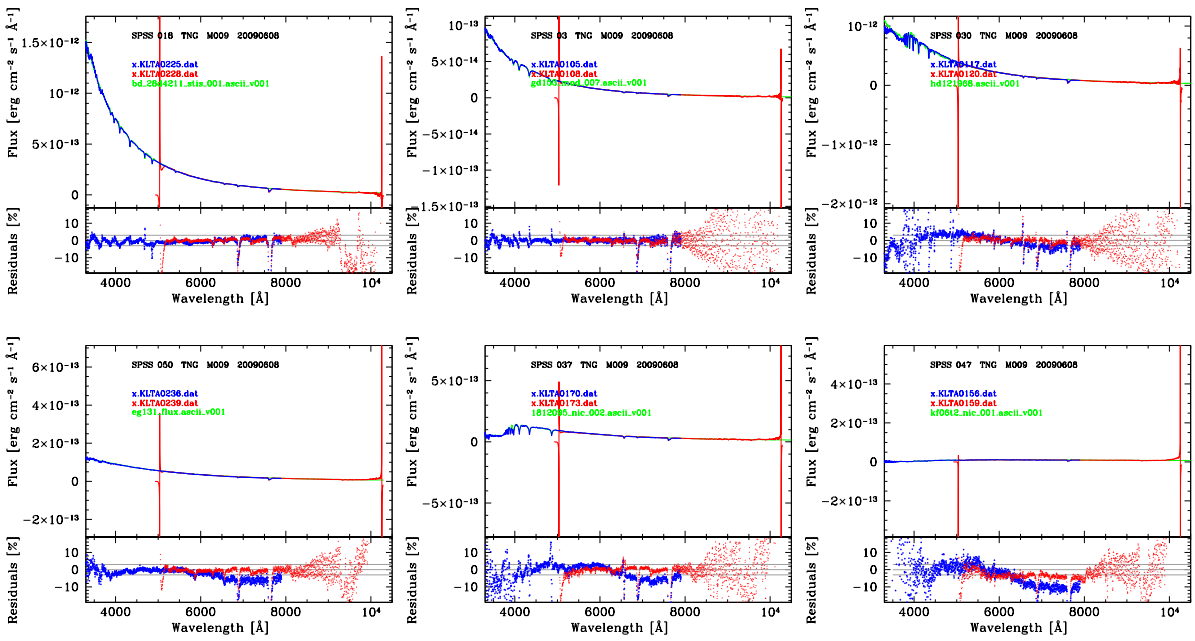

FIGURE 17: Spectra of SPSS sorted by spectral type, from the warmest to the coolest, from left to right and from top to bottom. In each panel, the LR-B spectra are plotted in blue, and the LR-R in red, with the lower sub-panels showing the residuals with respect to a literature reference template (in green in all upper sub-panels).

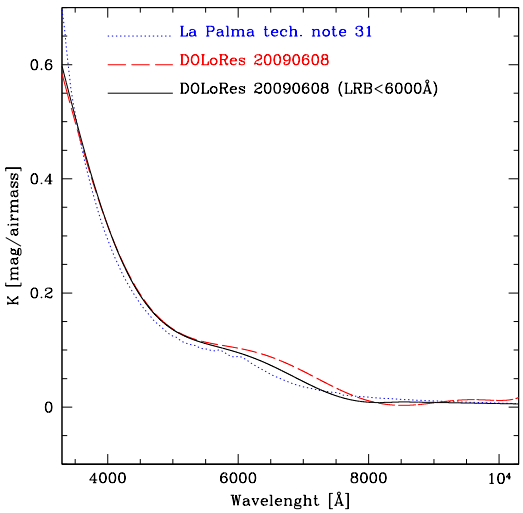

FIGURE 18: King (1985) extinction curve (blue dotted line), extinction curve derived using LR-B and LR-R spectra (red dashed line), extinction curve derived using LR-B spectra below 6000Å and LR-R spectra (black solid line).

The low polarization star HD154892[23] was observed with the same instrumental setup used for

[23] V=8.00, spectral type: F8V, B band polarization: 0.050%±0.030, see Turnshek et al. (1990).

the high polarized star, but at different position angles (-10, 45, 90 and 135 degrees) to check the effect of the internal instrumental polarization at the Nasmyth focus. Because of technical problems, no calibration lamps were acquired during the night.

Data reduction was performed as described in GCC-001.

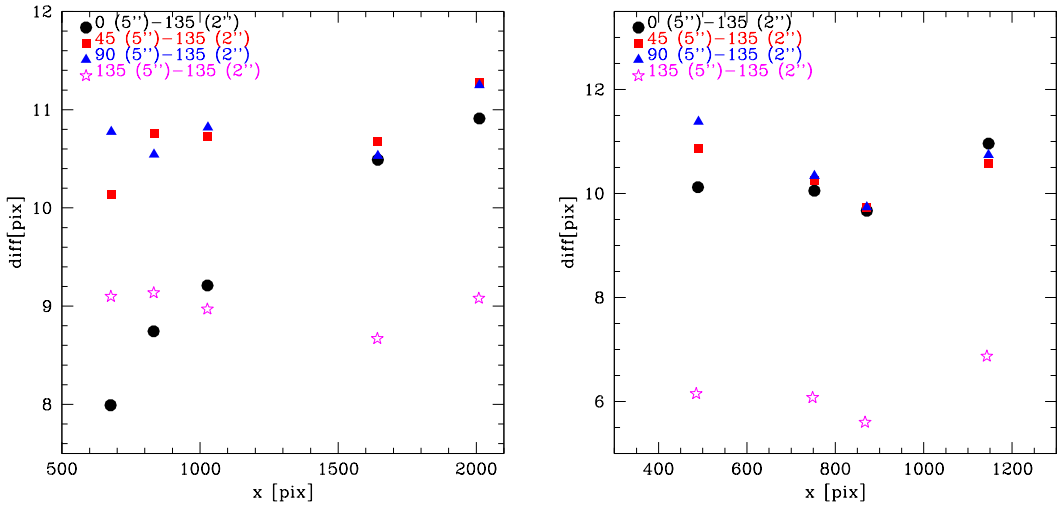

FIGURE 19: Offset (in Y axis, in pixel) of the LR-B (left panel) and LR-R (right panel) wide slit spectra observed at different position angles as a function of the position along dispersion (X axis, in pixels) with respect to the narrow slit spectrum. The LR-B dispersion is 2.52 Å/pixels, LR-R dispersion is 2.61 Å/pixels.

One particular spectrum of the high polarization star HD155197 (LR-B, 5" slit, at angle 0) showed a non linear shift (in pixels) with respect to the narrow slit spectrum, as if having a different dispersion relation (see Fig. 24). We found no plausible explanation and thus we decided to consider it a spurious anomaly.

Differential light loss is expected to be very small due to the large slit (5" width) and the good seeing (average seeing $\simeq 1.3$", but $\simeq 2.5$" in the worst spectrum). Also atmospheric extinction correction is expected not to change significantly the results because the airmass is almost constant for all the spectra.
Anyway, we applied the extinction correction (we used the extinction presented by King 1985) and differential light loss correction, according to the recipe by Bellazzini (2007)[24].

The results for the high polarization star HD155197 are shown in Fig. 20. The LR-B spectra have a similar shape from 5500 Å to the red edge. In this wavelength range their ratio is 1 within

[24]The content of this internal document will be published in a forthcoming Protocol on Data Reduction. Simulations show that for a given ratio $R = SLIT/FWHM$ between the image FWHM and the slit width, light loss can be modelled and corrected, by dividing the spectrum by a third order polynomial $FF_N = a_0 + a_1\lambda + a_2\lambda^2 + a_3\lambda^3$ whose coefficients can be computed as described in Bellazzini (2007) who also provide a table with the coefficients for several typical values of R.

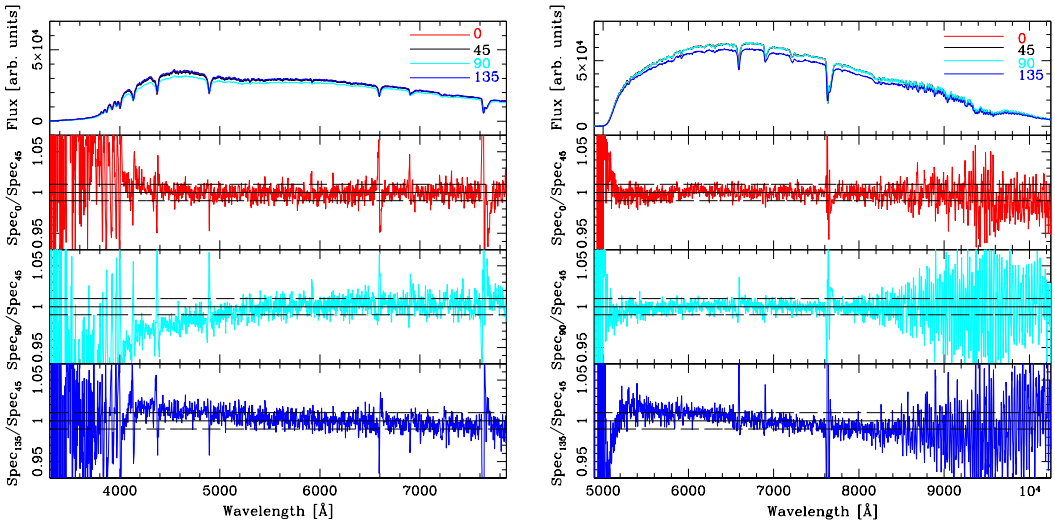

FIGURE 20: High polarization star HD155197, in the original experiment of May 26, 2008. Upper panels: LR-B and LR-R spectra observed at different position angle. Not all the spectra overlap because of variable sky transparency, nevertheless the global shape is preserved. Lower panels: LR-B and LR-R normalized ratio of the spectra taken with the 5" slit at angle 0, 90 and 135 degrees with respect to the spectrum taken at 45 degrees. A small shift in wavelength has been applied to better match the absorption lines. The dashed lines show the $\pm 1\%$ limits. Ratios have been normalized to 1 taking into account the values for $\lambda > 4500$ in the blue and $5500 < \lambda < 8500$ in the red.

1-2%. At shorter wavelengths there are larger deviations especially for the 90 deg spectrum, as if were too faint in the blue with respect to the reference spectrum. The 0-45 and 90-45 deg ratio of the LR-R spectra overlap very well within 1%, while the 135 spectrum shows a clearly non-flat trend. While in the blue the deviating spectrum is the one at 90 deg, in the red the deviating one is at 135 deg. The deviating spectra have in common the worst observing conditions: they are the faintest and they are characterized by the largest FWHM (twice the value measured for the other blue spectra, and $\simeq 1.5$ larger than the other red spectra, respectively).

The low polarized star HD154892 has been reduced in the same way as the high polarized star (but the wavelength calibration is based on the calibration lamps observed in the afternoon because of technical problems during the night and no differential light loss correction was applied because it was found negligible, of the order of $\sim 0.1\%$. Atmospheric extinction correction has been applied. The results are shown in Fig. 21. The hypothesis that flux differences are caused by veils and not by polarization effect is confirmed by a second test we performed under better sky conditions.

The results of the first test are the following:

- the spectra observed at different position angles show differences smaller than 1-2%

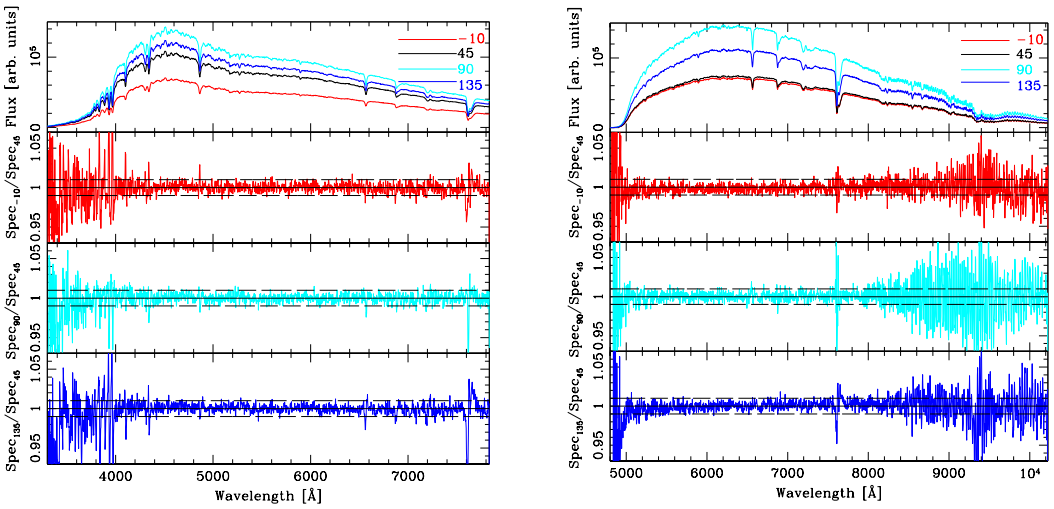

FIGURE 21: Low polarization star HD154892, in the original experiment of May 28, 2008. Upper panels: LR-B and LR-R spectra, naturally offset because of variable sky transparency (clouds). Lower panels: LR-B and LR-R normalized ratio of the spectra taken with the 5" slit at angle -10, 90 and 135 degrees with respect to the spectrum taken at 45 degrees. A small shift in wavelength has been applied to better match the absorption lines. The dashed lines show the $\pm 1\%$ limits. Ratios have been normalized to 1 taking into account the values for $4200 < \lambda < 7400$ in the blue and $5200 < \lambda < 10000$ in the red.

except at the blue noisy edge of the LR-B spectra and the red noisy edge of the LR-R spectra. The polarized star seems to show a slightly different spectral shape in the blue spectrum observed at 135 degrees, but still consistent with the other spectra within 2%. The corresponding red spectrum, that has about 1500 Å in common with the blue spectrum, shows a similar slope. The blue spectrum observed at 90 degrees shows a larger deviation (a few per cent) and it seems peculiar also on the 2D image. On the other hand the corresponding red spectrum shows a nice flat ratio with respect to the reference spectrum.
Since the faint deviating spectra correspond to the worst images and to different position angles (90 deg in the blue grism and to 135 deg in the red grism) we suspect that the reason of their anomaly is not due to polarization. However the reason of their trend is not clear, as well as the strange (larger) FWHM if compared to the other spectra.

- the analysis of the low polarized star spectra observed at different position angles does not show any significant correlation of the spectral shape with the angle. The overall shapes of the spectra agree with one another within 1% except at the blue edge (below 4000 Å), where the S/N is lower, and above 8000 Å, as expected because of fringing.

- the flux ratio of the faintest and the brightest spectra is equal to ~ 0.5, both in

the blue grism and in the red grism, because of clouds. The similar shape of the spectra observed under variable sky transparency is by the way a straightforward evidence that veils and thin clouds produce a grey extinction, as shown by Oke (1990), Pakštiene & Solheim (2003).

The analysed spectra of a polarized star do not show any dependence on the position angle, not even for those spectra with worse seeing or observed through veils, suggesting that the intrinsic polarization of a star has no significant impact ($> 3\%$) on the resulting spectral shape (excluding the borders, which are affected by low S/N or fringing). Nevertheless we repeated the the experiment[25] under better observing conditions and with a larger slit (10 arcsec instead of 5) to avoid differential light loss. The high polarization star HD155197 and the low polarization star HD154892 were spectroscopically observed again at 4 different position angles (-160, -108, -56, and -5 degrees and 170, 223, 274 and 325 degrees respectively), with grisms LR-B and LR-R. Spectra through the 2" slit were acquired for wavelength calibration, together with calibration arcs with the He and Ne+Hg+Ar+Kr lamps. The good seeing (0.8"–1.45") and the wide slit used ensure that all the flux is recovered. The comparison of the extracted spectra also shows that the sky transparency was constant along the test. Data has been reduced in the same way as in the first test, with the exception of the extinction curve (in this second test we used our own extinction curve[26] (which is very similar to the one used in the first test, given by King 1985). The results of this second test are shown in Figg. 22, 23.

The plots confirm that the anomalous results obtained in the first test are not a polarization effect and that indeed no significant correlation is found between the spectral shape and the position angle. The overall shapes of the spectra agree with one another within 1% except at the blue edge (below 4000 Å), where the S/N is lower, and above 8000 Å, as expected because of fringing. These new data also confirm that the flux differences noted in the first test are due to sky transparency variation, as supposed.

We also used the new data of HD155197 to build the same plots shown in Fig. 24, to check if all spectra have the same dispersion relation. One particular LR-B spectrum (the one at -5 deg) showed again a non linear shift (in pixels) with respect to the other spectra, as if having a different dispersion relation. As in the previous test, the anomalous spectrum was wavelength calibrated with arcs obtained for a different position angle, hence we suppose that the different behaviour can be the result of instrumental flexures (see also SMR-002). Because of our standard observing procedure includes calibration arcs at the same position of the corresponding spectra, this problem should not affect scientific data.

[25] TNG staff courtesy.
[26] ExtCurveLaPalma20090608.dat.

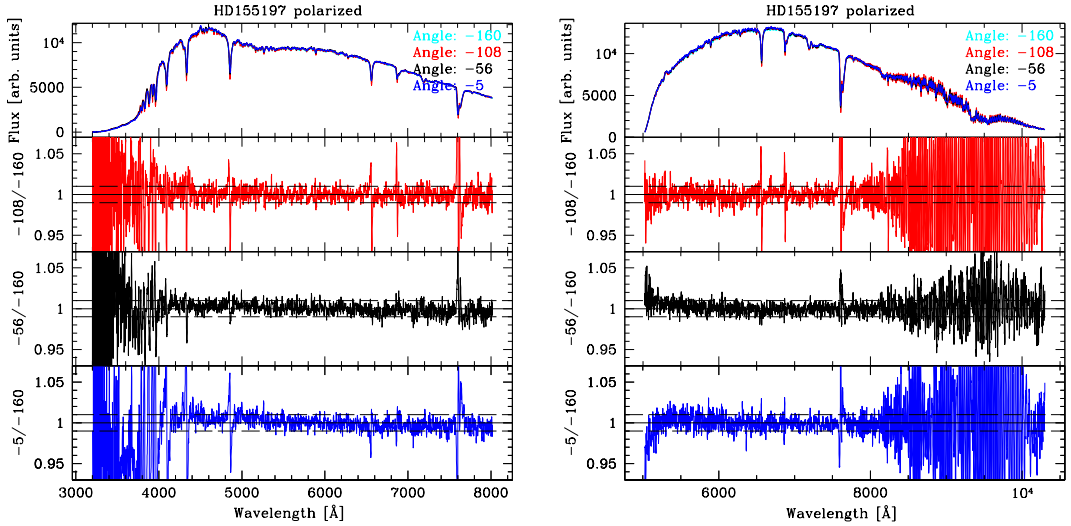

FIGURE 22: High polarization star HD155197, repeated on June 01, 2012. Upper panels: LR-B and LR-R spectra. Lower panels: LR-B and LR-R normalized ratio of the spectra taken with the 10" slit at angle -108, -56 and -5 degrees with respect to the spectrum taken at -160 degrees. The dashed lines show the $\pm 1\%$ limits. Ratios have been normalized to 1 taking into account the values for $\lambda > 4500$ in the blue and $5500 < \lambda < 8500$ in the red.

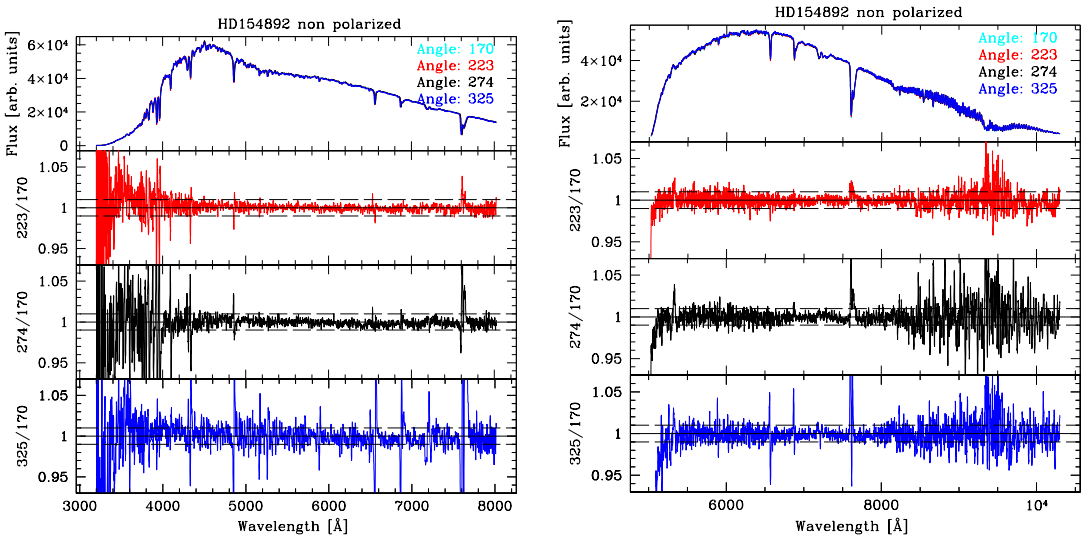

FIGURE 23: Low polarization star HD154892, repeated on June 01, 2012. Upper panels: LR-B and LR-R spectra, Lower panels: LR-B and LR-R normalized ratio of the spectra taken with the 10" slit at angle 223, 274 and 325 degrees with respect to the spectrum taken at 170 degrees. The dashed lines show the $\pm 1\%$ limits. Ratios have been normalized to 1 taking into account the values for $\lambda > 4500$ in the blue and $5500 < \lambda < 8500$ in the red.

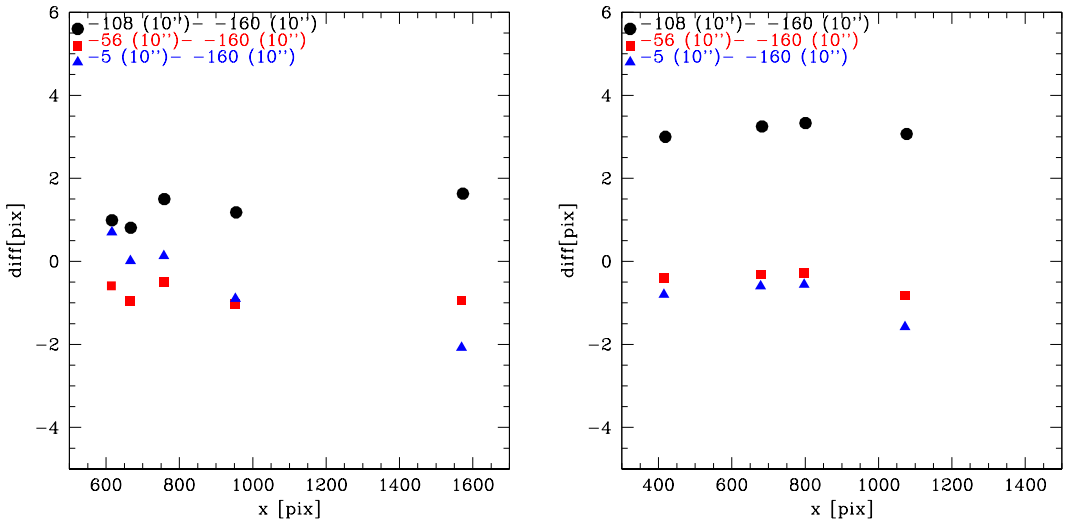

FIGURE 24: Offset (in Y axis, in pixel) of the LR-B (left panel) and LR-R (right panel) spectra observed at different position angles as a function of the position along dispersion (X axis, in pixels) with respect to a reference spectrum. The LR-B dispersion is 2.52 Å/pixels, LR-R dispersion is 2.61 Å/pixels.

4.3 DOLoRes Conclusions

The second order contamination of the LR-R spectra seems to start above $\simeq 9500$ Å. The second order blocking filter integrated in the LR-R grism greatly attenuates the contamination but does not suppress it completely. A simple linear relation, based on the little information extracted from the available data, mapping the second order spectrum on the first (eq. 10) is used to reduce the contamination. The C1, C2 curves and the percentage of the first order spectrum falling in the second one can be found in Wiki-Bo[27]. Because of the uncertain second order dispersion law and to the fact that the second order contamination wavelength range completely coincides with a strong H_2O absorption band, the correction is not always satisfactory.
The analysis of the LR-B spectra also shows a possible second order contamination, starting from ~ 6000Å. Because the LR-B contaminated range is covered by LR-R spectra, we suggest to cut the LR-B spectra at ~ 6000Å. If the second order contamination will be confirmed, a second order blocking filter would not be the best solution because the rejected wavelength range (probably below ~ 4000Å), could not be replaced by LR-R (while it is possible for wavelength larger than 6000Å), and it would be more convenient to keep the whole spectra and cut the contaminated section. Also the correction, similar to the LR-R second order correction, would be hard because based on a problematic wavelength range (presumably 3000–4000Å).

The analysed spectra of a polarized star do not show any dependence on the position angle, not even for those spectra with worse seeing or observed through veils, suggesting that the intrinsic

[27] http://yoda.bo.astro.it/wiki/index.php/Spectroscopy_Reduction_and_Analysis

polarization of a star has no significant impact (>1%) on the resulting spectral shape (larger deviations are visible at the spectra edges, probably due to low S/N and/or fringing).

Also the unpolarized star spectra agree with one another within 1%. The good overall match of the spectra suggests that the instrumental polarization effects are negligible with respect to the position angle and wavelength.

5 CAFOS@CAHA 2.2m

5.1 CAHA second order

According to the CAFOS on-line manual[28] the grism B200 (3200-7000 Å) is contaminated by the second order at wavelengths longer than 6500 Å; the R200 grism (6300-11000 Å) is contaminated at wavelengths longer than 10000 Å. The B200 contamination is not an issue, because the same wavelength range is observed with the red setup, moreover the analysis of the observed spectra did not show any significant contamination. We checked the contamination of the red setup using B200 and R200 spectra of a blue star (GD71). As shown in Fig. 25 a second order spectrum is visible in the R200 spectrum, but starting above 12100 Å, and hence it does not overlap the first order in our range of interest. In order to check that the observed "spurious" spectrum is really the second order, we compared the skylines observed in this region with the corresponding ones in the first order of the red spectrum and in the blue spectrum. We determined the first order skylines probably corresponding to the second order observed skylines, by visually inspecting the 2-dimensional spectra. The initial guess was checked by overplotting the sky lines of the first and second order, as shown in Fig. 25, right image. Indeed, two bright skylines seem to coincide in all spectra, but due to the shifting and stretching applied to compare them, the results may not be conclusive. Hence we compared the star spectrum in the same wavelength range, but due to the absence of strong features, the comparison turned out to be useless (Fig. 26, left image). We then compared the calibration arcs acquired with the B200 and R200 grisms, using the shifts and scale factors similar to the ones used to compare the skylines and the spectra. The result is shown in Fig. 26, right image. The coincidence of three lines confirms that the initial guess on the second order spectrum was correct.

The comparison of the wavelengths of the features identified in Fig. 26, right panel, measured after the wavelength calibration of the calibration arcs, allowed us to determine the function that maps the first order into the second order (see Tab. 4 and Fig. 27).

The linear fit of our data (Tab. 4, Fig. 27) gives us the following relation:

$$\lambda_{2^{nd}ord} = -465.6 + 2.049\lambda_{1^{nd}ord}$$

with a residual of $\sigma = 0.76$ Å. The second order, starting above 12100 Å is well separated from

[28] http://w3.caha.es/alises/cafos/cafos22.html

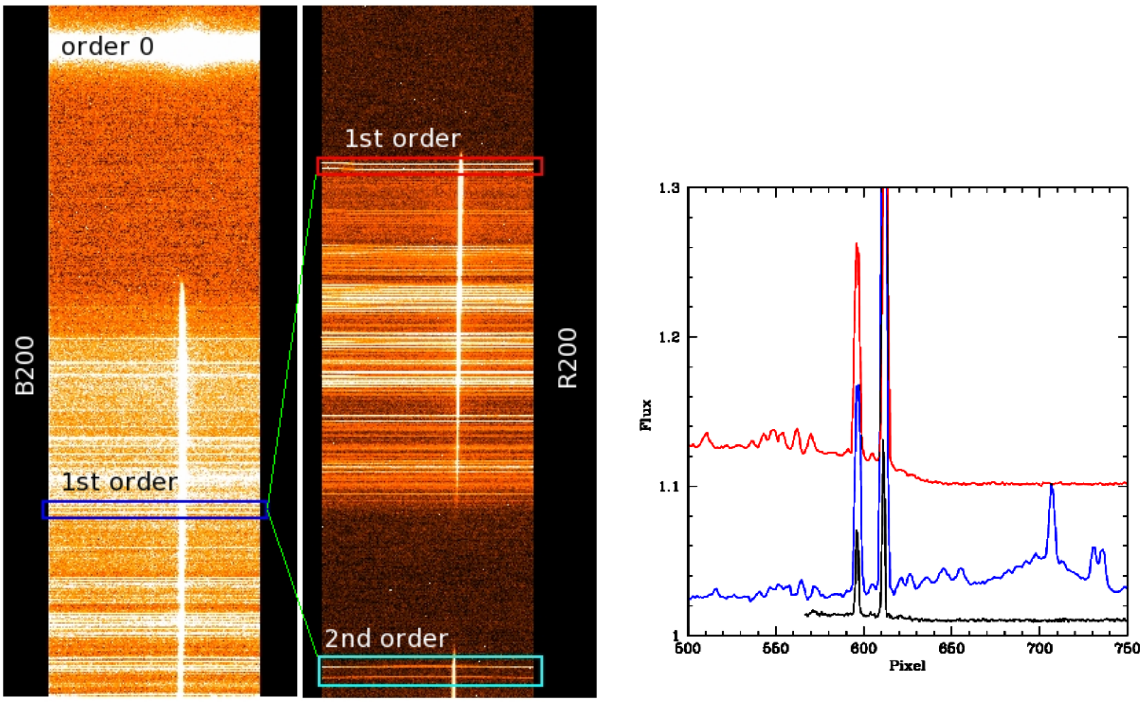

FIGURE 25: Left panel: Grism B200 (left) and R200 (right) spectrum of GD71 (slit 2") taken on Sept 21, 2011 by the CAHA staff. The B200 spectrum shows the zeroth and the first order, while the R200 spectrum shows the first and second orders. In both spectra, two bright sky lines are marked (in blue on the B200 spectrum and in cyan on the R200 spectrum). Right panel: a plot of the bright sky lines just mentioned: the blue line shows the B200 sky features, the red line shows the R200 sky features, scaled, shifted, and stretched to compare with the blue one. The black line shows the second order skylines, scaled, shifted, and stretched to be compared with the blue one.

TABLE 4: Position of the same emission lines in the B200 and R200 1^{st} order, and in the R200 2^{nd} order calibration arcs.

Element λ	1^{st} order, B200 [Å]	1^{st} order, R200 [Å]	2^{nd} order, R200 [Å]
Ar II 6232.89	6233.37	6234.28	12310.0
Cd I 6325.16	6325.01	6324.92	12496.5
Cd I 6438.47	6437.89	6438.58	12728.9

the first one, hence the second order contamination is not a problem. We note that the second order spectrum visible in the R200 spectra corresponds to the spectral range 6150–6450 Å.

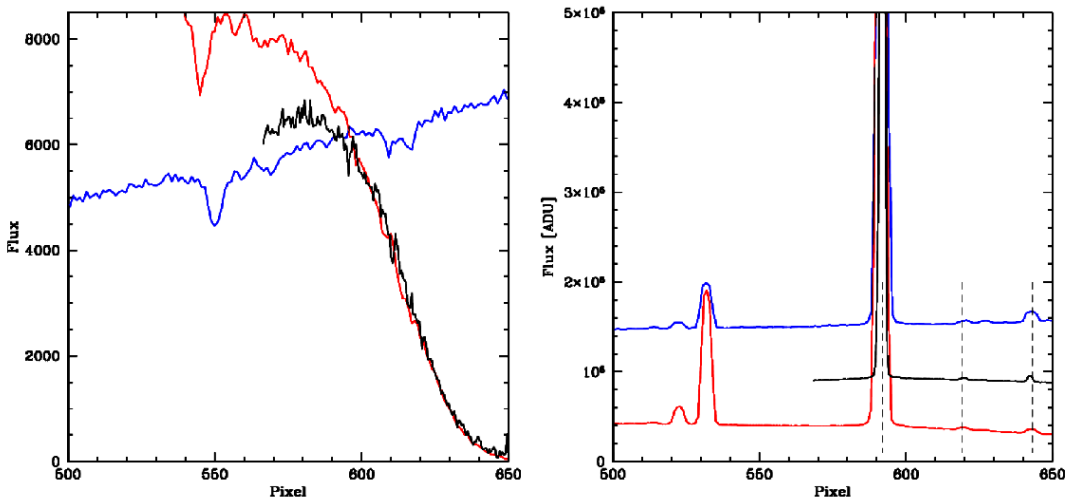

FIGURE 26: Left image: the blue line shows the B200 spectrum, the red line shows the R200 spectrum. The black line shows the second order spectrum. No features can be recognized on the second order spectrum. Right image: the blue line shows the B200 wavelength calibration lamp (HgCd, He, Rb), the red line shows the R200 wavelength calibration lamp features. The black line shows the second order wavelength calibration lamp. In this case three features, marked by dashed lines, can be recognized on all spectra, confirming that the spectrum labelled in Fig. 25 is indeed the second order spectrum. In both figures the red spectrum and the second order spectrum were scaled, shifted, and stretched to compare with the blue one. The examined regions are the ones corresponding to the bright skylines marked in Fig. 25.

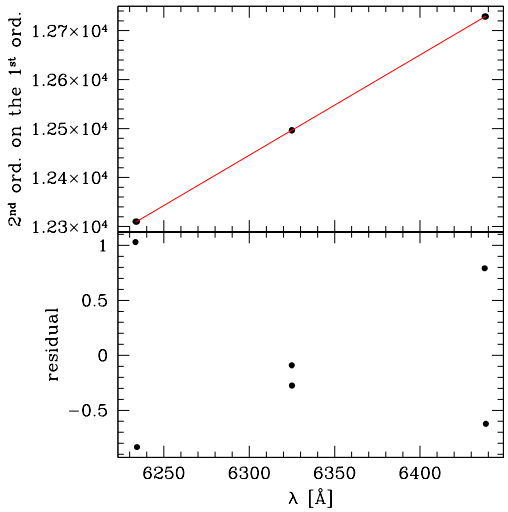

FIGURE 27: Linear fit of the first-second order relation.

5.2 CAHA polarization

Due to the optical telescope configuration, no significant polarization is expected (see Sec. 1.2).

5.3 CAHA Conclusions

The instrumental setup used in our observing campaign (B200 and R200) does not need any second order contamination correction.
Due to the optical telescope configuration, polarization is not expected to affect our data.

6 Conclusions

Table 5 summarizes the results obtained for the telescope-instrument combinations used in our survey and analysed in this document.

The second order contamination is absent or negligible in grism 3 and 5 at BFOSC@Cassini, in grism R200 and B200 at CAFOS@CAHA 2.2m and in grism 16 at EFOSC2@NTT. The second order contamination is moderate in grism LR-R at DOLoRes@TNG and more relevant in grism 11 at EFOSC2@NTT. We found hints of a possible faint second order contamination in grism LR-B at DOLoRes@TNG. Using the method described in Sec. 1.1.1 and a set of special observations, we produced C1 and C2, the response curves of light issuing from the first and second order, respectively. Applying these curves to any observed spectrum, by means of equations 6 and 7, the contamination can be strongly reduced, as described in Sec. 1.1.1.

Following the reasoning in Sec. 1.2, no instrumental polarization is expected in BFOSC@Cassini and CAFOS@CAHA 2.2m. We expect instead some instrumental polarization effect in DOLoRes@TNG and in EFOSC2@NTT. A test performed at TNG (see Sec. 4.2) shows that for normal spectroscopic observations of unpolarized stars (that is our case) the effect, if any, is always lower than 1% on average. The analyzed spectra of a polarized star show no clear dependence on the instrumental polarization, with deviation always lower than 2% (at most).

TABLE 5: Second order contamination & polarization for the telescope/instruments used in the absolute calibration programme of the Gaia spectro-photometric data

Telescope	Instrument	Second order contamination	Instrumental polarization	Ref.
Cassini 1.5m	BFOSC	GR3, none	negligible	Sec. 2.3
		GR5, none	negligible	Sec. 2.3
ESO NTT	EFOSC2	GR11, none	negligible	Sec. 3.3
		GR16, from 6000 Å, relevant	negligible	Sec. 3.3
TNG	DOLoRes	LR-B, from 6000 Å, faint	negligible	Sec. 4.3
		LR-R, from 9500 Å, moderate	negligible	Sec. 4.3
CAHA 2.2m	CAFOS	B200, from 6500 Å, negligible	negligible	Sec. 5.3
		R200, none	negligible	Sec. 5.3

7 References

[GA-001], Altavilla, G., Bellazzini, M., Pancino, E., et al., 2007, *The Primary standards for the establishment of the GAIA Grid of SPSS. Selection criteria and a list of candidates.*,
GAIA-C5-TN-OABO-GA-001,
URL http://www.rssd.esa.int/cs/livelink/open/2736914

[GA-003], Altavilla, G., Bragaglia, A., Pancino, E., et al., 2010, *Secondary standards for the establishment of the Gaia Grid of SPSS. Selection criteria and a list of candidates.*,
GAIA-C5-TN-OABO-GA-003,
URL http://www.rssd.esa.int/cs/livelink/open/3033479

[GA-002], Altavilla, G., Federici, L., e Pancino, E., et al., 2010, *Absolute calibration of Gaia spectro-photometric data. III. Observing facilities for ground-based support*,
GAIA-C5-TN-OABO-GA-002,
URL http://www.rssd.esa.int/cs/livelink/open/3012989

[GA-004], Altavilla, G., Pancino, E., Marinoni, S., et al., 2011, *Instrument Familiarization Plan for ground based observations of SPSS. I. CCD Shutter Characterization and Linearity Evaluation*,
GAIA-C5-TN-OABO-GA-004,
URL http://www.rssd.esa.int/cs/livelink/open/3075673

[GA-006], Altavilla, G., Cocozza, G., Ragaini, S., et al., 2013, *Data Reduction Protocol for Ground Based Observations of SpectroPhotometric Standard Stars. IV. Spectroscopy reductions up to relative flux calibration*,
GAIA-C5-TN-OABO-GA-006,
Draft

Bellazzini, M., 2007, gaia internal report

Bohlin, R., Lindler, D., Riess, A., 2005, Grism Sensitivities and Apparent Non-Linearity

Bohlin, R.C., Colina, L., Finley, D.S., 1995, AJ, 110, 1316, ADS Link

Breckinridge, J.B., Oppenheimer, B.R., 2004, ApJ, 600, 1091, ADS Link

[GCC-001], Cocozza, G., Altavilla, G., Carrasco, J.M., et al., 2013, *Data Reduction Protocol for Ground Based Observation of Spectrophotometric Standard Stars. II. Spectroscopy Pre-reduction up to extraction and wavelength calibration*,
GAIA-C5-TN-OABO-GCC-001,
URL http://www.rssd.esa.int/cs/livelink/open/3143422

[LF-001], Federici, L., Bragaglia, A., Diolaiti, E., et al., 2006, *Absolute calibration of Gaia photometric data. II. Observing facilities for ground-based support (pilot program)*,

GAIA-C5-TN-OABO-LF-001,
URL http://www.rssd.esa.int/cs/livelink/open/2706141

Giro, E., Bonoli, C., Leone, F., et al., 2003, In: S. Fineschi (ed.) Society of Photo-Optical Instrumentation Engineers (SPIE) Conference Series, vol. 4843 of Society of Photo-Optical Instrumentation Engineers (SPIE) Conference Series, 456–464, ADS Link

Gutierrez-Moreno, A., Heathcote, S., Moreno, H., Hamuy, M., 1994, PASP, 106, 1184, ADS Link

Hamuy, M., Walker, A.R., Suntzeff, N.B., et al., 1992, PASP, 104, 533, ADS Link

Hamuy, M., Suntzeff, N.B., Heathcote, S.R., et al., 1994, PASP, 106, 566, ADS Link

Høg, E., Fabricius, C., Makarov, V.V., et al., 2000, A&A, 355, L27, ADS Link

King, D., 1985, RGO/ La Palma technical note no 31

Landolt, A.U., 1992, AJ, 104, 372, ADS Link

Landolt, A.U., Uomoto, A.K., 2007, AJ, 133, 768, ADS Link

Lasker, B.M., Lattanzi, M.G., McLean, B.J., et al., 2008, AJ, 136, 735, ADS Link

[SMR-003], Marinoni, S., Pancino, E., Altavilla, G., et al., 2011, *Data Reduction Protocol for Ground Based Observations of SpectroPhotometric Standard Stars. III. Quality Control on SPSS Photometric Frames and Photometric Catalogues Production*,
GAIA-C5-TN-OABO-SMR-003,
Draft

[SMR-004], Marinoni, S., Bellazzini, M., Pancino, E., Altavilla, G., Cocozza, G., 2012, *Data Reduction Protocol for Ground Based Observations of SpectroPhotometric Standard Stars. IV. Short Variability Monitoring: Light Curves production and analysis*,
GAIA-C5-TN-OABO-SMR-004,
Draft

[SMR-001], Marinoni, S., Pancino, E., Altavilla, G., et al., 2012, *Data Reduction Protocol for Ground Based Observations of SpectroPhotometric Standard Stars. I. Imaging Pre-reduction*,
GAIA-C5-TN-OABO-SMR-001,
URL http://www.rssd.esa.int/cs/livelink/open/3117618

[SMR-002], Marinoni, S., Galleti, S., Cocozza, G., et al., 2013, *Instrument Familiarization Plan for ground based observations of SPSS. II. Calibration Frames Study and Recommendations*,
GAIA-C5-TN-OABO-SMR-002,
URL http://www.rssd.esa.int/cs/livelink/open/3198487

Oke, J.B., 1990, AJ, 99, 1621, ADS Link

Pakštiene, E., Solheim, J.E., 2003, Baltic Astronomy, 12, 221, ADS Link

[EP-001], Pancino, E., Altavilla, G., Bellazzini, M., et al., 2008, *Protocol for Ground Based Observations of SpectroPhotometric Standard Stars. I. Instrument Familiarization Tests*, GAIA-C5-TN-OABO-EP-001, URL http://www.rssd.esa.int/cs/livelink/open/2858529

[EP-003], Pancino, E., Altavilla, G., Carrasco, J.M., et al., 2009, *Protocol for Ground Based Observations of SpectroPhotometric Standard Stars. II. Variability Searches and Absolute Photometry Campaigns Photometry Campaigns*, GAIA-C5-TN-OABO-EP-003, URL http://www.rssd.esa.int/cs/livelink/open/2908205

Reach, W.T., Megeath, S.T., Cohen, M., et al., 2005, PASP, 117, 978, ADS Link

Sánchez-Blázquez, P., Peletier, R.F., Jiménez-Vicente, J., et al., 2006, MNRAS, 371, 703, ADS Link

Schroeder, D.J., 2000, *Astronomical optics*, San Diego: Academic Press

Szokoly, G.P., Bergeron, J., Hasinger, G., et al., 2004, ApJS, 155, 271, ADS Link

Traub, W.A., 1990, Journal of the Optical Society of America A, 7, 1779, ADS Link

Turnshek, D.A., Bohlin, R.C., Williamson, R.L., II, et al., 1990, AJ, 99, 1243, ADS Link